Potent antitumor activity of anti-HER2 antibody-topoisomerase I inhibitor conjugate based on self-immolative dendritic dimeric-linker

Potent antitumor activity of anti-HER2 antibody-topoisomerase I inhibitor conjugate based on self-immolative dendritic dimeric-linker

Yulia Liubomirski[1], Galia Tiram[1], Anna Scomparin[1,2], Samer Gnaim[3], Sayantan Das[3], Sachin Gholap[3], Liang Ge[3], Eilam Yeini[1], Omri Shelef[3], Arie Zauberman[4], Nir Berger[4], Doron Kalimi[4], Mira Toister-Achituv[4], Christian Schröter[5], Stephan Dickgiesser[5], Jason Tonillo[5], Min Shan[5], Carl Deutsch[5], Stanley Sweeney-Lasch[5], Doron Shabat[*3], Ronit Satchi-Fainaro*[1,6]

[1] Department of Physiology and Pharmacology, Sackler Faculty of Medicine, Tel Aviv University, Tel Aviv 6997801, Israel.

[2] Department of Drug Science and Technology, University of Turin, Turin, 10125 Italy.

[3] School of Chemistry, Raymond and Beverly Sackler Faculty of Exact Sciences, Tel Aviv University, Tel Aviv 6997801, Israel.

[4] Inter-Lab, a subsidiary of Merck KGaA, South Industrial Area, Yavne 8122004, Israel

[5] Merck KGaA, Darmstadt, 64293 Germany

[6] Sagol School of Neuroscience, Tel Aviv University, Tel Aviv 6997801, Israel.

*Authors to whom correspondence should be addressed:

Prof. Ronit Satchi-Fainaro, Ph.D.

Department of Physiology and Pharmacology, Sackler Faculty of Medicine, Tel Aviv University, Ramat Aviv, Tel Aviv 6997801, Israel.

Tel: 972-3-6407427,

E-Mail: ronitsf@tauex.tau.ac.il

Prof. Doron Shabat, Ph.D.

Department of Organic Chemistry, School of Chemistry,

Raymond and Beverly Sackler Faculty of Exact Sciences,

Tel Aviv University, Ramat Aviv, Tel Aviv 6997801, Israel.

E-Mail: chdoron@post.tau.ac.il

Keywords

Antibody-Drug Conjugate (ADC), Belotecan, Breast Cancer, Dendritic Linker, Dimeric Prodrug, Exatecan, HER2, Trastuzumab

Abstract

Antibody-drug conjugates (ADCs) are a rapidly expanding class of anticancer therapeutics, with 14 ADCs already approved worldwide. We developed unique linker technologies for the bioconjugation of drug molecules with controlled-release applications. We synthesized cathepsin-cleavable ADCs using a dimeric prodrug system based on a self-immolative dendritic scaffold, resulting in a high drug-antibody ratio (DAR) with the potential to reach 16 payloads due to its dendritic structure, increased stability in the circulation and efficient release profile of a highly cytotoxic payload at the targeted site. Using our novel cleavable linker technologies, we conjugated the anti-human epidermal growth factor receptor 2 (anti-HER2) antibody, trastuzumab, with topoisomerase I inhibitors, exatecan or belotecan. The newly synthesized ADCs were tested *in vitro* on mammary carcinoma cells overexpressing human HER2, demonstrating a substantial inhibitory effect on the proliferation of HER2-positive cells. Importantly, a single dose of our trastuzumab-based ADCs administered *in vivo* to mice bearing HER2-positive tumors, showed a dose-dependent inhibition of tumor growth and survival benefit, with the most potent antitumor effects observed at 10 mg/kg, which resulted in complete tumor regression and survival of 100% of the mice. Overall, our novel dendritic technologies using the protease-cleavable Val-Cit linker present an opportunity for the development of highly selective and potent controlled-released therapeutic payloads. This strategy could potentially lead to the development of novel and effective ADC technologies for patients diagnosed with HER2-positive cancers. Moreover, our proposed ADC linker technology can be implemented in additional medical conditions such as other malignancies as well as autoimmune diseases that overexpress targets, other than HER2.

Introduction

Human epidermal growth factor receptor 2 (HER2) is overexpressed in a broad number of cancer types, including breast, ovarian, colorectal, gastric, head and neck, and liver cancers[1, 2]. Specifically, in breast cancer, HER2 is overexpressed in ~15-30% of patients, due to amplification or activating somatic mutations of gene encoding HER2 (ERBB2), closely correlating with poor prognosis and poor overall survival rates, thus, presenting an attractive candidate for targeted therapeutic applications[3, 4]. Trastuzumab (Herceptin®) is a clinically approved HER2 humanized monoclonal antibody and a standard-of-care for HER2-positive early and advanced breast cancer and advanced gastric cancer, either as a single agent or in combination with chemotherapy[1, 5]. Although trastuzumab targeted therapy transformed the treatment of HER2-positive cancers, many patients treated with trastuzumab-based therapy gradually develop resistance, and some experience severe side-effects such as cardiotoxicity, especially when combined with anthracycline-based chemotherapy treatment[6, 7].

The design of novel treatments with superior anti-tumor efficacy and reduced off-target toxicities continues to be a clinical challenge. Targeted therapy, using small molecules or biologics, has gained significant attention in the last decade[8, 9]. One special class of targeted therapy is antibody-drug conjugates (ADCs) which are a rapidly growing class of anti-cancer therapeutics, representing a unique opportunity to increase the safety of highly toxic drugs by utilizing the specificity of antibodies to obtain targeted delivery of potent cytotoxic molecules to specific tissues. Currently, there have been 14 ADCs approved for marketing worldwide for the treatment of hematological malignancies and solid tumors[10] and over 100 ADC candidates in different stages of clinical development. Specifically, for HER2-positive tumors, trastuzumab has been effectively exploited to target cytotoxic agents directly to HER2-expressing cancers, as illustrated by the US Food and Drug Administration (FDA) approval of two trastuzumab-based ADCs, Ado-trastuzumab emtansine (Kadcyla®; T-DM1) and fam-trastuzumab deruxtecan-nxki (Enhertu®; T-DXd).

Much of the success of ADCs is attributed to technological advances made in the design of the linker between the antibody and the therapeutic payloads. The linker

technology employed has a significant impact on balancing between ADC therapeutic efficacy and off-target toxicity[17, 18]. Thus, several key linker properties should be addressed when designing efficient and selective ADCs. Ideal ADCs should present high stability in circulation to limit the premature release of toxic agents in the bloodstream and off-target compartments, high water solubility to aid bioconjugation and prevent the formation of ADC aggregates, and should efficiently release highly cytotoxic payloads at desired targeted sites[18]. Furthermore, homogenous conjugation of the ADC contributes to its efficacy. Broader DAR distribution produces more heterogenous ADC, which results in product inconsistency and suboptimal efficiency[19]. *In vivo* studies have shown improved therapeutic window and tolerability of developed ADCs with DAR2 with high homogeneity (>90%)[20].

The vast majority of ADCs in clinical development employ cleavable linkers with specific release mechanisms to allow the controlled release of solitary drug molecules at the target site[21]. Considering that each conjugation site between an antibody and a linker has the potential to impact the antibody's binding affinity with its antigen, it would be advantageous to explore the development of linkers with cleavage sites capable of initiating the release of multiple drug molecules upon a single cleavage event. Another key component of ADCs is the cytotoxic payload. Due to the fact that only a low fraction of ADCs administered reach their target, and the drug loading capacity on the antibody is limited, highly potent drugs are required for effective ADCs. Moreover, as ADC technology is highly selective to its target, it allows the use of highly potent drugs that could not have been used in their free unbound form. Currently, the main cytotoxic drugs incorporated in ADCs under clinical development include microtubule inhibitors and DNA targeting agents, some of which could not have been used as free drugs due to their toxicity and/or hydrophobicity[22].

Here we report an efficient construction of novel trastuzumab-based ADCs using self-immolative dendritic prodrug dimeric-platform for bioconjugation of topoisomerase I inhibitor compounds, exatecan or belotecan, to trastuzumab. Our novel dendritic-based linker system enables the conjugation of two drugs per linking site and utilizes the intrinsic properties of the tumor cells in the context of a protease-mediated linker cleavage. The valine-citrulline (Val-Cit) dipeptide present in the linker is recognized

and processed predominantly by lysosomal proteases, such as cathepsins, which are overexpressed in cancer cells, thereby enabling accurate and selective payload release at the tumor site[23]. Furthermore, we have incorporated a short solubilizing enhancer moiety in order to increase the aqueous solubility of the hydrophobic structure. Dendritic prodrugs that are activated through a single catalytic reaction by a specific enzyme offer advantage in augmenting tumor growth inhibition, especially if the targeted or secreted enzyme exists at relatively low levels in the malignant tissue. In addition, by attachment of a dimeric-prodrug unit, the number of conjugation sites on the antibody molecule is reduced by a factor of 2-fold to reach the same drug-to-antibody ratio (DAR) and a higher DAR can be achieved.

Herein, we evaluated the anti-tumor potential of our ADCs with exatecan or belotecan payloads at DAR4 (*i.e.,* 2 linkers carrying 4 drug molecules) and compared their therapeutic efficacy to T-DXd (DAR8) in HER2-positive breast cancer model. In general, trastuzumab-exatecan dendrimer ADC demonstrated higher anti-tumor activity than belotecan and similar therapeutic potential to T-DXd despite bearing half the number of drug molecules attached to the antibody.

Materials and Methods

Prodrug synthesis

Detailed synthetic schemes, chemical preparation and experimental procedures of the linker-drug used in this study, are provided in the **Supplementary Data** section.

Preparation of antibody-drug conjugates (ADCs)

Exatecan-based prodrug 1 or belotecan-based prodrug 2 were conjugated to trastuzumab (Herceptin®; Roche PZN-10816760) using a two-step chemoenzymatic approach as described by Dickgiesser *et al.*[24]. In a first step, thiol-bearing cysteamine (2-amino-ethanetiol) was enzymatically conjugated to trastuzumab using a microbial transglutaminase (MTG) specifically addressing glutamine 295 in both antibody heavy chains (EU numbering). The two conjugated cysteamine moieties served as handles for the attachment of thiol-reactive prodrugs 1 (exatecan prodrug) and 2 (belotecan

prodrug) in a second step resulting in ADCs trastuzumab-exatecan (Tras-Exa; DAR4): Trastuzumab-Thiol spacer at Q295-Dendron-Cat B-cleavable linker (Val-Cit)-Exatecan; trastuzumab-belotecan (Tras-Bel; DAR4): Trastuzumab-Thiol spacer at Q295-Dendron-Cat B-cleavable linker (Val-Cit)-Belotecan, respectively.

Drug-linker Gly-Gly-Phe-Gly(GGFG)-DXd was conjugated to trastuzumab or rituximab (Roche 10179132-02; PZN-08709904) targeting endogenous antibody cysteine residues as described previously[25]. Briefly, antibodies were incubated with 10 molar equivalents of tris(2-carboxyethyl)phosphine for disulfide reduction. Afterwards, 16-18 molar equivalents of prodrug 3 (DXd prodrug; see Supplementary Data **Figure S26**) were added for attachment to reduced cysteine thiols generating trastuzumab-deruxtecan (T-DXd; DAR8): Trastuzumab-Maleimide-GGFG-DXd or rituximab-deruxtecan (Ritux-DXd; DAR8): Rituximab-Maleimide-GGFG-DXd ADCs.

Conjugates were purified by size-exclusion chromatography using HiLoad™ 16/600 Superdex™ 200 pg columns (Cytiva) and 10 mM Histidine, 3 % Trehalose, 100 mM NaCl, pH 5.5 as running buffer. ADCs were analyzed using reversed phase chromatography (RP-HPLC; PLRPS column, 4000 Å, 5 µm, 2.1 × 50 mm, Agilent technologies) and analytical size exclusion chromatography (SE-HPLC; TSKgel SuperSW3000 column, 4.6 x 300 mm, Tosoh Bioscience) as described previously[24]. For liquid chromatography mass spectrometry (LC-MS) DAR determination, ADCs were diluted with 0.1 % formic acid to a final concentration of 0.05 mg/mL. Subsequently, 100 µL of this solution were reduced with 1 µL TCEP (500 mM) for 5 min at room temperature. LC-MS analysis was performed using an Exion HPLC system (Buffer A: 0.1% formic acid in water (Biosolve, 23244101), Buffer B: 0.1% formic acid in acetonitrile (Biosolve, 01934101) coupled to a Sciex 6600+ mass spectrometer by a Turbo V ESI source. 4 µl protein solution was loaded onto an Phenomenex bioZen 3.6 µm Intact C4 column (50 x 2.1 mm) and eluted with a linear gradient from 15 % to 95 % Buffer B within 3 min and 0.25 mL/min flow rate. Data were acquired in IDA mode with positive polarity, in a mass range from 400 to 4000 m/z. Other instrument settings were as follows: source voltage 5.5 kV, declustering potential 180 V, accumulation time 1 s, source temperature 450 °C, gas1 50 L/h, and gas2 25 L/h. The mass spectrometer was calibrated with ESI positive calibration solution 5600.

Acquired data were processed with Genedata Expressionist 16.5. All the ADCs used in this study were conjugated in house as described above. The serum stability assay was performed using the commercial Enhertu® (please see below).

Serum stability

The serum stability assay was conducted as previously described[26, 27] applying some minor modifications: Tras-Exa (DAR4), Tras-Bel (DAR4) and trastuzumab-deruxtecan [T-DXd, Enhertu® (Daiichi Sankyo; NDC 65597-406-01; Asaman, MA, USA); DAR8: Trastuzumab-Maleimide-(GGFG)-DXd] conjugates were incubated at a final concentration of 5 µM conjugated payload (considering the DAR of each construct) in human and mouse serum (Biowest). Moreover, serum samples were supplemented with 5 µM deuterated 7-Ethyl-d3-camptothecin (D3-CPT) as an internal standard.

Pharmacokinetics study

For pharmacokinetic (PK) study plan concerning animal care have been reviewed by the RBM Designated Veterinarian. Protection of animals used, housing and welfare are guaranteed according to the Italian D.Lvo. No. 26 of March 4, 2014. Physical facilities for accommodation and care of animals are in accordance with the provisions of the Italian D.Lvo. 2014/26 and of Directive 2010/63/EU. The Institute is fully authorized by Italian Ministry of Health.

C57BL/6 wild type mice and hu FcRn transgenic mice were purchased from Charles River Laboratories (Italia Srl, Via Indipendenza, 11 - 23885 Calco). ADCs were administered to the animals (n=6/group) at 3 mg/kg single dose, by intravenous injection. Mice were divided (n=3/time point) and 70 µL of blood samples were collected from mice #1, 2, 3 at 0.08, 24, 72, 240, and 504 h and from mice #4, 5, 6 at 4, 48, 168 and 336 h after dosing. Plasma samples were tested by using an immunoassay method for the quantification of total human IgG antibodies in mouse sera for all groups. The lower limit of quantification (LLOQ) of total antibodies was 50 ng/mL and values below the LLOQ were considered 0 ng/mL for descriptive statistics and necessary condition analysis (NCA). PK analysis was performed using Phoenix WinNonlin® version 6.3 (Pharsight Corporation, USA) with a non-compartmental (model independent) approach.

Cell lines

HCC-1954, and MDA-MB-468 human mammary carcinoma cells were obtained from the American Type Culture Collection (ATCC, Manassas, VA, USA). JIMT-1 cells were obtained from the German Collection of Microorganisms and Cell Cultures GmbH (DSMZ). HCC-1954 and JIMT-1 cells were cultured in Dulbecco's modified Eagle's medium (DMEM; Gibco) supplemented with 10% fetal bovine serum (FBS; Gibco), 100 IU/mL penicillin, 100 µg/ml streptomycin, 12.5 U/mL nystatin, 2 mM L-glutamine and 100 µg/mL sodium pyruvate (Biological Industries, Israel). MDA-MD-468 cells were cultured in Roswell Park Memorial Institute 1640 (RPMI-1640; Gibco) supplemented with 10% FBS, 100 IU/mL penicillin, 100 µg/mL streptomycin, 12.5 U/mL nystatin, 2 mM L-glutamine. All cells were grown at 37°C in 5% CO_2. All experiments were performed with mycoplasma-free cells. All human cell lines were purchased within the last three years and hence, were authenticated using STR profiling by the ATCC.

HER2 quantification

For each sample, $0.8x10^6$ cells (HCC1954, JIMT-1 or MDA-MB-468) were prepared in 50 µL of Dulbecco's phosphate-buffered saline (DPBS)x1 containing 1% bovine serum albumin (BSA; #BAH65; Equitech-Bio). Trastuzumab was added to a final concentration of 100 nM. The sample was incubated on ice for 45 min. A wash step was performed with 2 mL of cold DPBS + 1% BSA, the sample was spun down and supernatant was discarded. The detection antibody (AlexaFluor 488 $F(ab')_2$ Donkey Anti-human IgG-Fc) (#709-546-098; Jackson ImmunoResearch Laboratories) was added in a volume of 80 µL and incubated for 30 min on ice. Cells were then washed twice in DPBS + 1% BSA, resuspended in 500 µL of DPBSx1 and then taken for flow cytometry analysis (BD FACSAria™ III). Analysis was done using the FCS Express™ software (De Novo Software).

A calibration curve was prepared for each cell line, according to manufacturer's instructions of the Quantum™ Simply Cellular anti-human IgG kit (Bangs Laboratories Inc.), using the trastuzumab (Herceptin®) antibody and the same detection antibody that was used for the experiments.

HER2-ADC binding assay

For each sample $0.8x10^6$ cells (HCC1954, JIMT-1 or MDA-MB-468) were prepared in 50 µL of DPBSx1 + 1% BSA. The following ADCs and antibodies were added to a final concentration of 100 nM: T-DXd (DAR8), Tras-Exa (DAR4), Tras-Bel (DAR4), Isotype control Ritux-DXd and trastuzumab. The samples were incubated on ice for 45 min. A wash step was performed with 2 mL of cold DPBS + 1% BSA, centrifugation and supernatants were discarded. The detection antibody (AlexaFluor 488 $F(ab')_2$ Donkey Anti-human IgG-Fc) was added in a volume of 80 µL, and incubated for 30 min on ice. Cells were then washed twice in DPBS + 1% BSA, resuspended in 500 µL of DPBSx1 and then taken for flow cytometry analysis, in a BD FACSAria™ III. Analysis was done using the FCS Express™ software (De Novo Software).

Cell viability assay

HCC-1954, JIMT-1 and MDA-MB-468 cells were plated in 24-well culture plates (5000, 5000 and 10,000 cells/well, respectively) and incubated for 24 h. Cells were then exposed to serial dilutions of trastuzumab, free exatecan, or Tras-Exa (DAR4) ADC. Cell viability was evaluated following 6 days incubation using MTT (3 µg/mL, Sigma). MTT absorbance was measured at 570 nm using SpectraMax M5e multi-detection reader.

***In vivo* study**

All animals were housed in the Tel Aviv University Specific Pathogen Free (SPF) animal facility. The experiments were approved by the animal care and use committee (IACUC) of Tel Aviv University (approval no. 01-19-088) and conducted in accordance with NIH guidelines.

HCC-1954 cells ($1x10^6$) were injected into the mammary fat pad of 6-weeks old female severe combined immune deficient (SCID) mice. Tumor growth was monitored by caliper and the volume was defined as 0.52 x width x $length^2$. When tumor volume reached approximately 95 mm^3, mice were randomized into groups (n=9/group) and intravenously injected with a single dose of T-DXd (DAR8), Tras-Exa (DAR4) or Tras-Bel (DAR4), at three different concentrations (1, 3 or 10 mg/kg). As controls, mice were treated either with 10 mg/kg of Ritux-DXd (DAR8) or with a vehicle control (10 mM Histidine, 3% Trehalose, 100 mM NaCl, pH 5.5). All treatments were administered

at a volume of 200 µL/20 g mouse. Mice were euthanized when tumor volume reached 1000 mm^3, when tumors became necrotic and/or ulcerated, or when mice lost 15% of their body weight.

Statistical analyses

Data is presented as mean ± standard error of mean (SEM), unless stated otherwise. The statistical significance in overall survival was determined with a log-rank (Mantel-Cox) test using GraphPad Prism 9 software. Statistical significance was defined as $p < 0.05$.

Results and Discussion

Molecular design, bioconjugation, and characterization of ADCs

Almost 20 years ago, we have demonstrated the ability of *para*- and *ortho*-quinone-methide eliminations to occur consecutively on the same aromatic phenol or aniline derivative, by the introduction of proper leaving groups on such positions[28]. This double elimination mechanism is initiated by the removal of the head-substrate and formation of a phenol or an aniline intermediate, which then undergoes p-quinone-methide elimination to release the first reporter group; this is followed by o-quinone-methide elimination to release the second reporter. Incorporation of drug molecules as the tail units and an enzyme substrate as the trigger generated a dimeric-prodrug unit that was activated upon a single enzymatic cleavage. This self-immolative dendritic scaffold enables attachment and then consecutive release of two identical or different chemotherapeutic drugs[29-31].

In this work, we synthesized a new dimeric prodrug system based on an AB2 self-immolative dendritic scaffold, where exatecan (red) is the chemotherapeutic drug and Val-Cit dipeptide is used as a substrate for cathepsin B (**Fig. 1A; prodrug 1,** see **Supplementary Data Figures S1-S24** for detailed synthesis). A maleimide moiety (brown) was introduced at the focal site in order to enable conjugation to an antibody molecule *via* reaction with a thiol functionality (thiol functional groups were introduced via glutamine modification using transglutaminase ligation with cysteamine). In addition, a short solubilizing moiety, composed of tetra-carboxylate

(blue), was attached to the dendritic prodrug scaffold in order to increase the aqueous solubility of the hydrophobic structure. The self-immolative dendritic linker, when paired with two copies of exatecan, creates a molecular structure that is extremely hydrophobic, rendering it insoluble in water. Consequently, these dendritic molecules cannot be effectively conjugated with an antibody, as the highly lipophilic system undergoes complete precipitation in aqueous media. The inclusion of a hydrophilic unit in the para-position of the AB2 self-immolative dendritic linker dramatically improved the hydrophilicity of this molecular system and thus enabled sufficient water solubility to allow conjugation with the antibody. Furthermore, trials using a solubilizing unit on the dendritic linker, which is less hydrophilic than the current one, resulted in aggregation of the ADC molecules.

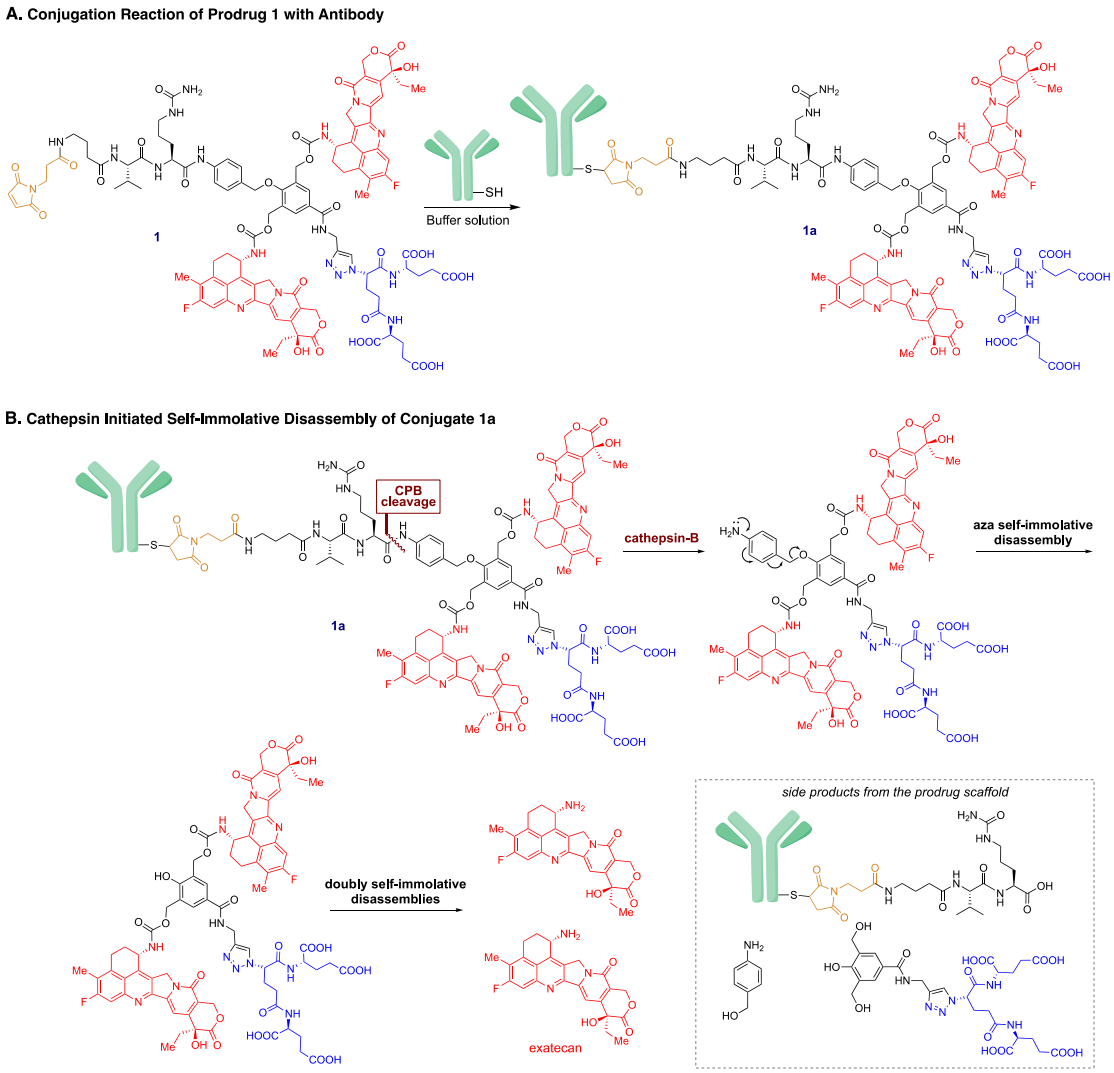

Figure 1. (A) Conjugation of prodrug 1 to an antibody. Cysteamine was attached to antibodies using microbial transglutaminase (MTG) which was then conjugated with

exatecan self-immolative dimeric prodrug *via* thiol-maleimide chemistry (see Methods). The Buffer solution for the antibody conjugation of drug-linker was PBS, 1 mM EDTA, pH 7.4. **(B) Cathepsin-B initiated self-immolative disassembly of conjugate 1a**. The release mechanism of the two exatecan drug molecules from the ADC system by cathepsin B. PBS - Phosphate, buffered saline; CPB - cathepsin B.

The release mechanism of the two exatecan drug molecules from the ADC system is presented in **Figure 1B**. The prodrug disassembly is initiated by enzymatic cleavage of the specific amide bond between the Val-Cit dipeptide and the aniline linker by cathepsin B. The generated aniline undergoes aza-quinone-methide elimination to release a phenol intermediate, which then undergoes two consecutive quinone-methide eliminations to release the two exatecan chemotherapeutic drug molecules.

The belotecan dimeric prodrug 2 was synthesized in an analogue manner to that described for the exatecan prodrug (**Fig. S25**).

Prodrugs 1 and 2 were conjugated to trastuzumab using a site-specific, chemoenzymatic two-step conjugation strategy to generate ADCs Tras-Exa and Tras-Bel, respectively, carrying two dimeric prodrugs, hence four drugs per antibody. T-DXd and Ritux-DXd were produced by attaching prodrug 3 (**Fig. S26**) directly to endogenous antibody cysteines to yield ADC with DARs around 8. A slightly higher DAR of 4.3 for Tras-Exa indicated some unspecific conjugation, but overall the anticipated DARs could be reached, and analytical size-exclusion chromatography (SEC) analysis revealed high purity for all four ADCs (**Table 1, Fig. S27**).

Table 1. Generated ADCs and key data.

Antibody + prodrug	ADC	DAR	Purity (%)
Trastuzumab + Val-Cit-Exatecan dendrimer [prodrug 1]	Tras-Exa	4.3	97.8
Trastuzumab + Val-Cit-Belotecan dendrimer [prodrug 2]	Tras-Bel	3.9	99.7
Trastuzumab + GGFG-DXd [prodrug 3]	T-DXd	7.9	96.3
Rituximab + GGFG-DXd [prodrug 3]	Ritux-DXd	8.0	99.0

DAR values were determined by LC-MS and refer to the total number of cytotoxic drugs (each prodrug 1 or 2 accounts for two drugs). Purity values were determined by SE-HPLC and calculated by dividing the peak area of the monomeric species by the overall area including high and low molecular weight species.

In vitro serum stability, binding and cytotoxicity of Tras-Exa/Bel ADCs

First, we assessed the linker-drug stability of our trastuzumab-based ADCs in serum. To this end, Tras-Exa (DAR4), Tras-Bel (DAR4) and T-DXd (DAR8) were monitored overtime for their payload release in mouse (**Table 2, Fig. S28**) and human (**Table 2, Fig. S28**) serum by the detection of free exatecan, belotecan and DXd *via* LC-MS/MS. Following 96 h incubation of the ADCs in sera, minimal amounts of the conjugated payload were released from both Tras-Exa and Tras-Bel ADCs in mouse (0.4% and 0.2%, respectively) and human (0.3% and 0.2%, respectively) sera after. Similarly, we analyzed control ADC-bearing exatecan at DAR4 *via* Val-Cit linker in mouse, monkey and human serum and monitored for changes in the DAR. Following incubation of the ADC in different serum samples at 37°C for 96 h, the mean DAR remained stable over time at ~4 (**Fig. S29**). Overall, these data indicated that our ADCs are highly stable while maintaining the desired DAR. Moreover, as many preclinical studies are performed using murine systems, linker stability is of great importance when evaluating the therapeutic potential of new drugs, specifically in such models. These results demonstrated superior stability in mice for our dimeric Val-Cit linker compared to the classic monomeric Val-Cit linker, previously reported to exhibit a very short half-life of 2.3 h in mouse plasma[32].

Table 2. Drug-linker stability.

	Free payload (% of total payload)			
ADC	**Mouse serum**		**Human serum**	
	0 h	**96 h**	**0 h**	**96 h**
T-DXd	0.2	1.9	0	1.3
Tras-Exa	0	0.4	0	0.3
Tras-Bel	0	0.2	0	0.2

Percentage of ADC remaining over time in mouse and human sera following incubation at 37°C for 96 h, calculated from free exatecan, belotecan or DXd that were measured *via* LC-MS/MS. Numbers show the released fraction (%) relative to initially conjugated payload.

Prior to evaluating our trastuzumab-Exa/Bel conjugates for their anti-tumor effects *in vitro* and *in vivo*, we confirmed the expression levels of HER2 in two different HER2-positive human breast cancer cell lines used in this study. In line with previous reports, which classified HCC-1954 as HER2 medium/high-expressing cells and JIMT-1 as low-

expressing cells[33, 34], cell surface quantification of HER2 on HCC-1954 and JIMT-1 cell showed approximately 1,700,000 and 190,000 receptors per cell, respectively (**Fig. 2A**). In comparison, the HER2-negative breast cancer cell line MDA-MB-468[35] showed 777 HER2 receptors per cell (which might be below the limit of detection of the kit used) (**Fig. 2A**).

Next, while it is not expected that the conjugation of prodrugs to the heavy chains of trastuzumab will affect its ability to bind HER2, we validated the binding ofTras-Exa/Bel ADCs, unconjugated naked trastuzumab (Herceptin®) and T-DXdin an *in vitro* cellular antigen-binding assay using flow cytometry. Considering the potential limitation of such an assay when comparing ADCs with different Fc regions, linkers and drugs, we used the same detection antibody. This analysis showed that at fixed concentration of 100 nM, the three ADCs and naked trastuzumab bound similarly to HER2-positive cells, with no difference in binding ability detected due to the use of different linkers and/or payloads. Binding of all trastuzumab-based antibodies to HCC-1954 cells was higher than to JIMT-1 cells, correlating with their respective HER2 expression levels (**Fig. 2B1,2B2**). Moreover, no binding of either antibody was observed in the HER2-negative MDA-MB-468 cells (**Fig. 2B3**).

These results suggest that the bioconjugation techniques used to generate Tras-Exa and Tras-Bel ADCs, did not impair the quaternary structure or masked the complementarity-determining regions of trastuzumab, resulting in intact binding of the antibodies to their target on the tumor cells, as compared to the naked trastuzumab.

In correlation with the previous HER2 expression experiment, *in vitro* cytotoxicity assay showed that HCC-1954 cells were significantly more sensitive to Tras-Exa compared to MDA-MB-468 (**Fig. 2C1,2C3**). Furthermore, Tras-Exa had a lower IC_{50} compared to free exatecan in HCC-1954 cells (**Fig. 2C1,2C4**). Moreover, Tras-Exa did not show any advantage compared to free exatecan in JIMT-1 cells (**Fig. 2C2**). This may be attributed to lower HER2 expression levels in JIMT-1 compared to HCC-1954, demonstrating the correlation of our trastuzumab-based ADC and HER2 levels. Of note, Tras-Exa showed some cytotoxic effects in MDA-MB-468 cells (**Fig. 2C3,2C4**). While cathepsins are normally associated with intracellular lysosomal activity, it has

been shown that cathepsin B is also secreted into the extracellular matrix by cancer cells, including breast tumor cells[36]. Thus, in such *in vitro* settings, HER2-negative cells might be affected by exatecan cleaved from the ADC, regardless of the HER2-directed delivery of the therapeutic agent. Moreover, mechanisms of target-independent uptake mediated by non-specific endocytosis may also contribute to such off-target toxicity[37].

A. HER2 extracellular quantitation

	HCC-1954	JIMT-1	MDA-MB-468
Amount of HER2/cell	1,707,241	189,082	777

B. HER2-ADC binding

B1. HCC-1954 (HER2+++)

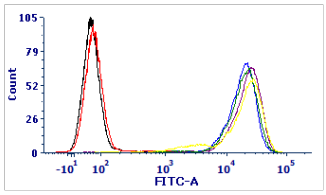

Antibody	MFI
AlexaFluor 488	53.56
Ritux-DXd	62.83
T-DXd	17084.09
Tras-Exa	20823.51
Tras-Bel	17919.94
Trastuzumab	19737.37

B2. JIMT-1 (HER2+)

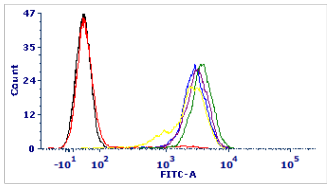

Antibody	MFI
AlexaFluor 488	33.99
Ritux-DXd	38.11
T-DXd	2509.08
Tras-Exa	2770.70
Trast-Bel	3312.48
Trastuzumab	2182.57

B3. MDA-MB-468 (HER2-)

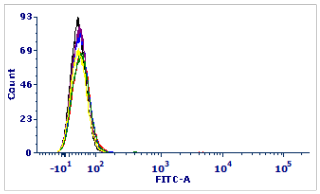

Antibody	MFI
AlexaFluor 488	29.87
Ritux-DXd	39.14
T-DXd	36.05
Tras-Exa	33.99
Tras-Bel	38.11
Trastuzumab	31.93

C. Cytotoxicity

C1. HCC-1954 (HER2+++)

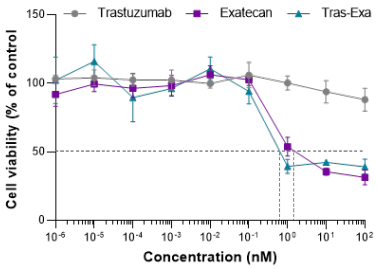

C2. JIMT-1 (HER2+)

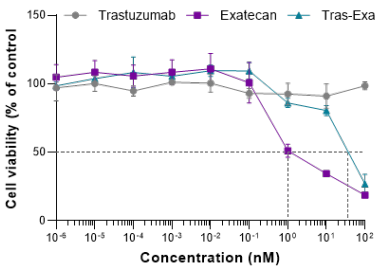

C3. MDA-MB-468 (HER2-)

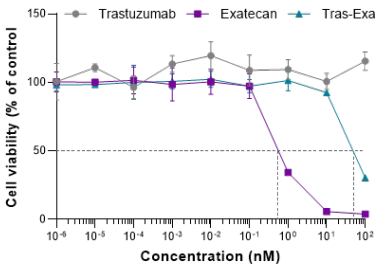

C4. IC_{50} (nM)

	HCC-1954	JIMT-1	MDA-MB-468
Trastuzumab	N/A	N/A	N/A
Exatecan	1.5	1	0.6
Tras-Exa	0.6	40	50
Tras-Exa/Exa Fold change	**0.4**	**40**	**83**

Figure 2. ***In vitro*** **evaluation of Tras-Exa ADC**. **(A)** HER2 cell surface expression. Data represent the average values of n=2; **(B)** Trastuzumab and trastuzumab-based ADCs binding to HER2(+) HCC-1954 cells (B1), JIMT-1 cells (B2) and HER2(-) MDA-MB-468 cells (B3 data is representative of n=2); **(C)** Viability of HCC-1954 (C1), JIMT-1 (C2), and MDA-MB-468 (C3) cells following 144 h (6 days) treatment with serial dilutions of trastuzumab, exatecan or Tras-Exa. (C4) Table summarizing the IC_{50} values of the different treatments. Data represent mean ± SD. Data is representative of n=3.

Pharmacokinetic (PK) parameters and therapeutic efficacy in a HER2-positive breast cancer model

The PK parameters of control-ADC [isotype-Val-Cit-exatecan dendrimer (DAR4)] were assessed and compared to isotype-GGFG-DXd (DAR8) following a single intravenous administration at 3 mg/kg. For both ADCs no clear differences were observed and demonstrated similar PK profiles in both hu FcRn and C57BL/6 strains (**Fig. 3A**).

Finally, Tras-Exa ADC (DAR4) and Tras-Bel ADC (DAR4) were evaluated for their *in vivo* anti-tumor efficacy. To this end, mice bearing HCC-1954 xenografts were treated once with Tras-Exa or Tras-Bel at three doses (1, 3 and 10 mg/kg) and monitored for tumor growth and survival. The therapeutic efficacy of our ADCs was compared to T-DXd (DAR8), which was also administered at three doses (1, 3 and 10 mg/kg), and to an isotype control of Ritux-Dxd (DAR8), which was given only at the highest dose of 10 mg/kg. An additional control group was treated with the vehicle. A dose-dependent inhibition of tumor growth was observed, with the most potent antitumor effect observed at 10 mg/kg for the three trastuzumab-based ADCs (**Fig. 3B**). Interestingly, a single dose of Tras-Exa or T-DXd at the highest concentration (10 mg/kg) resulted in a complete tumor regression. Conversely, 4 out of 9 (44%) of the Tras-Bel-treated mice at 10 mg/kg, relapsed 60 days following treatment (**Fig. 3B1**). Furthermore, a moderate anti-tumor activity was observed at 3 mg/kg for all ADCs, with T-DXd demonstrating slightly stronger tumor growth inhibition among the different ADCs (**Fig. 3B2**). Overall, Tras-Exa and T-DXd showed a superior anti-tumor activity compared to Tras-Bel ADC at 3 and 10 mg/kg, with no statistically significant difference in efficacy between these two ADCs for both concentrations. In contrast, treatment with the lowest dose (1 mg/kg) had no impact on tumor growth compared to the controls in either ADC (**Fig. 3B3**). These results correlate with *in silico* outcomes using our newly-established prediction algorithm for ADC performance based on Shah *et al*.[38]

Of note, following treatments, mice of all experimental groups, including the vehicle and isotype control, exhibited transient body weight loss, which was recovered after 5 days (**Fig. 3B4**). Overall, our trastuzumb-based ADCs were well-tolerated at all doses evaluated, similarly to T-DXd, vehicle or isotype control, with net positive weight gain over the course of the study (**Fig. 3B4**).

A. Pharmacokinetic parameters

A1. C57BL/6

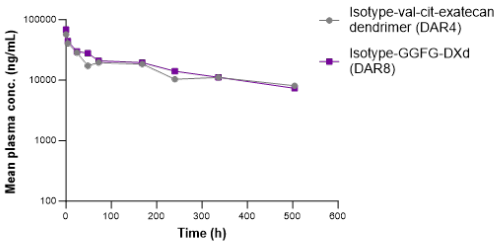

A2. hu FcRn

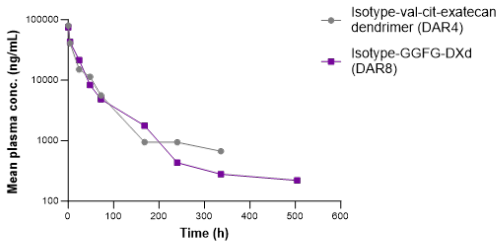

A3.

Strain	ADC	C_{last}	AUC_{last}	Ext	AUC_{INF}	Beta $t_{1/2}$	Cl		V_{ss}	
		(mg/mL)	(h*mg/mL)	(%)	(h*mg/mL)	(days)	(mL/h/kg)		(mL/kg)	
							Estimate	CV%	Estimate	CV%
hu FcRn	Isotype-GGFG-DXd (DAR8)	0.00067	1.67	2	1.7	2.74	1.76	4	112	2
hu FcRn	Isotype-val-cit-exatecan dendrimer (DAR4)	0.000221	1.77	0.8	1.79	3.49	1.68	4	104	2
C57BL/6	Isotype-GGFG-DXd (DAR8)	0.0081	7.94	30	11.1	11.67	0.270	7	107	1.5
C57BL/6	Isotype-val-cit-exatecan dendrimer (DAR4)	0.00737	8.11	30	11.1	11.79	0.270	10.6	103	3.2

B. *In vivo* antitumor activity

B1. 10 mg/kg

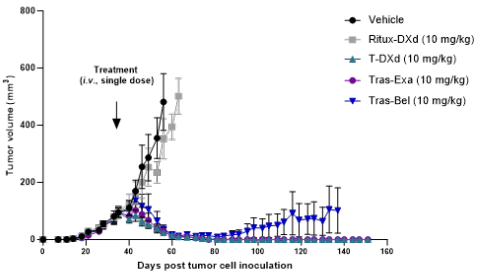

B2. 3 mg/kg

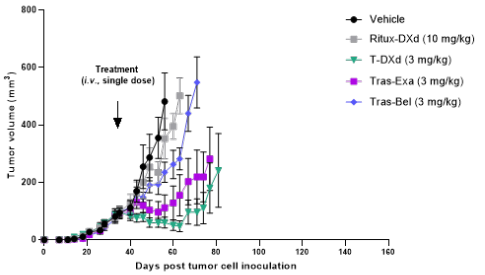

B3. 1 mg/kg

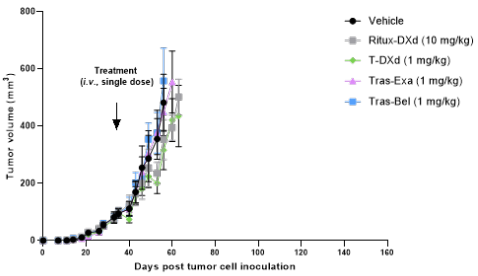

B4. Body weight change

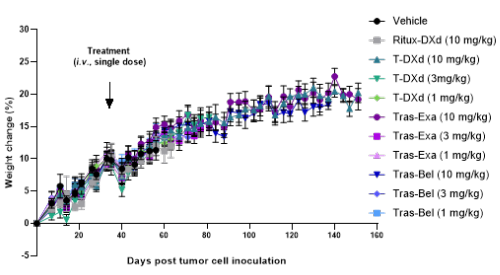

Figure 3. Trastuzumab-based ADCs lead to a dose-dependent inhibition of tumor growth. (A) PK parameters following a single intravenous administration of isotype-GGFG-DXd (DAR8) and isotype-Val-Cit-exatecan dendrimer (DAR4) at 3 mg/kg to two mice strains (hu FcRn and C57BL/6) for 21 days (n=3 mice/time point; in total n=6 mice/group). C_{last} – last measurable concentration; AUC_{last} – area under the curve up to the last quantifiable time-point; Ext – extrapolated; AUC_{Inf} – area under the curve extrapolated to the infinite time; Cl – clearance; V_{ss} – volume of distribution at steady state; CV – coefficient of variation. PK statistical analyses were done for AUC and Cl. Ext (%) calculated as the percent of the AUC that is extrapolated. **(B)** Growth curves of HCC1954 tumors following single intravenous injection of trastuzumab-based ADCs at three concentrations (n=9 mice/group): 10 mg/kg (B1); 3 mg/kg (B2) and 1 mg/kg (B3). All treatment groups were included in the same experiment; data are presented in separate graphs for clarity. **(B4)** Body weight change, expressed as percent change from the day of tumor cell inoculation. Data are presented as mean ± s.e.m.

In line with the data described above, Kaplan-Meier analyses demonstrated a dose-dependent survival benefit of the different ADCs evaluated. At the end of the study (day 152), 100% of mice treated with 10 mg/kg of Tras-Exa or T-DXd and 89% of mice treated with Tras-Bel at the same concentration were alive; while none of the control-treated mice survived past day 109 (vehicle) and 116 (Ritux-Dxd) (**Fig. 4A1,4B**). Moreover, treatment at 3 mg/kg significantly prolonged the median survival of mice treated with Tras-Exa (116 days) or T-DXd (137 days) compared to vehicle control (60 days) and Ritux-Dxd (71 days) (**Fig. 4A2,4B**). Tras-Bel (3 mg/kg) had no significant effect on mice survival compared to the controls, with a median survival of 84 days (**Fig. 4A2,4B**). At the lowest dose of 1 mg/kg, neither ADC showed any therapeutic efficacy in comparison to vehicle and isotype controls (**Fig. 4A3,4B**).

Overall Tras-Exa showed similar efficacy to T-DXd at 3 and 10 mg/kg despite having lower DAR of 4 compared to DAR8 of T-DXd.

A1. 10 mg/kg

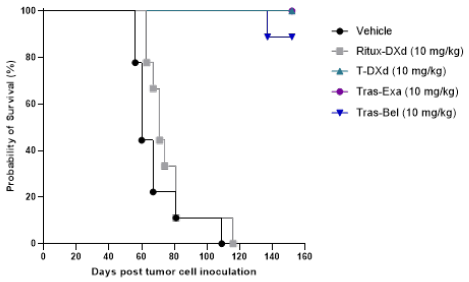

A2. 3 mg/kg

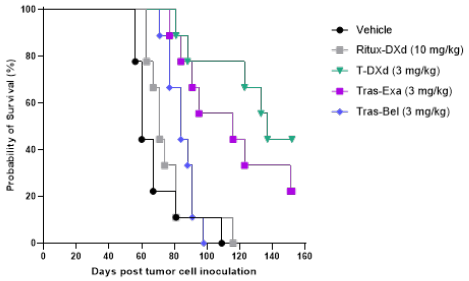

A3. 1 mg/kg

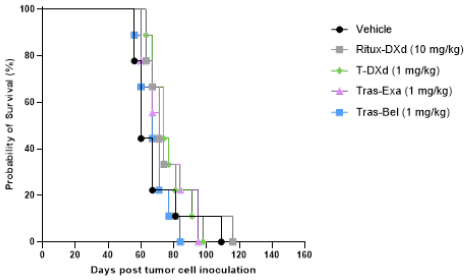

B.

Comparison of survival curves	Log-Rank (Mantel-Cox) test
Vehicle *vs.* **Ritux-DXd 10 mg/kg**	ns
Vehicle *vs.* **T-DXd 10 mg/kg**	<0.0001
Vehicle *vs.* **T-DXd 3 mg/kg**	<0.0001
Vehicle *vs.* **T-DXd 1 mg/kg**	ns
Vehicle *vs.* **Tras-Exa 10 mg/kg**	<0.0001
Vehicle *vs.* **Tras-Exa 3 mg/kg**	0.0007
Vehicle *vs.* **Tras-Exa 1 mg/kg**	ns
Vehicle *vs.* **Tras-Bel 10 mg/kg**	<0.0001
Vehicle *vs.* **Tras-Bel 3 mg/kg**	ns
Vehicle *vs.* **Tras-Bel 1 mg/kg**	ns
Ritux-DXd 10 mg/kg *vs.* **T-DXd 10 mg/kg**	<0.0001
Ritux-DXd 10 mg/kg *vs.* **T-DXd 3 mg/kg**	0.0001
Ritux-DXd 10 mg/kg *vs.* **T-DXd 1 mg/kg**	ns
Ritux-DXd 10 mg/kg *vs.* **Tras-Exa 10 mg/kg**	<0.0001
Ritux-DXd 10 mg/kg *vs.* **Tras-Exa 3 mg/kg**	0.0017
Ritux-DXd 10 mg/kg *vs.* **Tras-Exa 1 mg/kg**	ns
Ritux-DXd 10 mg/kg *vs.* **Tras-Bel 10 mg/kg**	<0.0001
Ritux-DXd 10 mg/kg *vs.* **Tras-Bel 3 mg/kg**	ns
Ritux-DXd 10 mg/kg *vs.* **Tras-Bel 1 mg/kg**	ns
T-DXd 10 mg/kg *vs.* **T-DXd 3 mg/kg**	0.0101
T-DXd 10 mg/kg *vs.* **T-DXd 1 mg/kg**	<0.0001
T-DXd 3 mg/kg *vs.* **T-DXd 1 mg/kg**	0.0002
Tras-Exa 10 mg/kg *vs.* **Tras-Exa 3 mg/kg**	0.0008
Tras-Exa 10 mg/kg *vs.* **Tras-Exa 1 mg/kg**	<0.0001
Tras-Exa 3 mg/kg *vs.* **Tras-Exa 1 mg/kg**	0.003
Tras-Bel 10 mg/kg *vs.* **Tras-Bel 3 mg/kg**	<0.0001
Tras-Bel 10 mg/kg *vs.* **Tras-Bel 1 mg/kg**	<0.0001
Tras-Bel 3 mg/kg *vs.* **Tras-Bel 1 mg/kg**	0.0016
T-DXd 10 mg/kg *vs.* **Tras-Exa 10 mg/kg**	ns
T-DXd 10 mg/kg *vs.* **Tras-Bel 10 mg/kg**	ns
Tras-Exa 10 mg/kg *vs.* **Tras-Bel 10 mg/kg**	ns
T-DXd 3 mg/kg *vs.* **Tras-Exa 3 mg/kg**	ns
T-DXd 3 mg/kg *vs.* **Tras-Bel 3 mg/kg**	0.0012
Tras-Exa 3 mg/kg *vs.* **Tras-Bel 3 mg/kg**	0.0076
T-DXd 1 mg/kg *vs.* **Tras-Exa 1 mg/kg**	ns
T-DXd 1 mg/kg *vs.* **Tras-Bel 1 mg/kg**	ns
Tras-Exa 1 mg/kg *vs.* **Tras-Bel 1 mg/kg**	ns

Figure 4. Trastuzumab-based ADCs prolong the survival of mice in a dose-dependent manner. (A) Kaplan–Meier overall survival curves of HCC-1954 tumor-bearing SCID mice treated intravenously with a single injection of trastuzumab-based ADCs at three concentrations (n=9 mice/group): 10 mg/kg (A1); 3 mg/kg (A2) and 1 mg/kg (A3). All treatment groups were included in the same experiment; data are presented in separate graphs for clarity. **(B)** Table summarizing the statistical significance of survival curves between different treatment groups, as analyzed using the log-rank (Mantel-Cox) test. $P < 0.05$; ns = not significant.

Conclusions

In this study, we developed a novel and highly effective trastuzumab-based HER2-targeting ADC using a new dimeric prodrug system based on an AB2 self-immolative dendritic scaffold. Our novel trastuzumab-exatecan ADC demonstrated high stability in serum while maintaining intact HER2 binding ability. Furthermore, our linker is more stable compared to conventional Val-Cit linkers, which show instability in mice, *i.e.* half-life of 2.3 h[32] *versus* ~70 days for our linker, according to the $t_{1/2}$ of our control ADC in mice (Data not shown). Importantly, trastuzumab-exatecan ADC exhibited a highly potent antitumor activity *in vivo* in HER2-positive breast cancer model, compared to the FDA-approved T-DXd (Enhertu®; DAR8) despite having half the DAR, *i.e.,* DAR4. Overall, our findings highlight the therapeutic potential of this novel trastuzumab-exatecan ADC as an effective option for the treatment of patients overexpressing HER2. Furthermore, our novel linker-drug technology has the potential to serve as a platform for further technological advances. It can potentially assist in the development of trastuzumab-based therapy given either as combination with a different active agent or as monotherapy ADCs using distinct payloads attached to the same antibody. Moreover, this linker technology can be employed in the development of novel ADCs for a wide array of molecular targets beyond HER2. Nevertheless, there is a need for further investigations of trastuzumab-exatecan ADC in a clinical setting.

Acknowledgements

The Satchi-Fainaro and Shabat laboratories received partial funding from Merck group. RSF received additional funding from the European Research Council (ERC) Advanced Grant Agreement no. [835227]-3DBrainStrom; The Israel Science Foundation (Grant No. 1969/18); and The Israel Cancer Research Fund (PROF-18-682).

Declaration of competing interests

RS-F is a Board Director at Teva Pharmaceutical Industries Ltd, relevant to work unrelated to this article. RS-F and DS received research funding from Merck.

Supplementary Data

General information

All reactions requiring anhydrous conditions were performed under an Argon atmosphere. All reactions were carried out at room temperature (RT) unless stated otherwise. Chemicals and solvents were either A.R. grade or purified by standard techniques. Thin-layer chromatography (TLC): silica gel plates Merck 60 F254: compounds were visualized by irradiation with UV light. Column chromatography (FC): silica gel Merck 60 (particle size 0.040-0.063 mm), eluent given in parentheses. Reverse-phase high-pressure liquid chromatography (RP-HPLC): C18 5u, 250x4.6mm, eluent given in parentheses. Preparative RP-HPLC: C18 5u, 250x21mm, eluent given in parentheses. 1H-NMR spectra were measured using Bruker Avance operated at 400 MHz. 13C-NMR spectra were measured using Bruker Avance operated at 101 MHz. Chemical shifts were reported in ppm on the δ scale relative to a residual solvent (CDCl3: δ = 7.26 for 1H-NMR and 77.16 for 13C-NMR, DMSO-d6: δ = 2.50 for 1H-NMR and 39.52 for 13C-NMR). Mass spectra were measured on Waters Xevo TQD. All general reagents, including salts and solvents, were purchased from Sigma-Aldrich.

Abbreviations

ACN - Acetonitrile, **CDI** - 1,1'-Carbonyldiimidazole, **DCC** - *N*, *N*'-Dicyclohexylcarbodiimide, **DCM** - dichloromethane, **DIPEA** - *N*,*N*-Diisopropylethylamine, **DMF** - *N*,*N*'-Dimethylformamide, **DMBA** - Dimethylbarbituric acid, **DMAP** - 4-(Dimethylamino)-pyridine, **DMSO** - Dimethyl sulfoxide, **EDC** - 1-Ethyl-3-(3-dimethylaminopropyl)-carbodiimide, **EEDQ** - N-Ethoxycarbonyl-2-ethoxy-1,2-dihydroquinoline, **EtOAc** - Ethylacetate, **HBTU** - 2-(1H-Benzotriazol-1-yl)-1,1,3,3-tetramethyluronium hexafluorophosphate, **Hex**- Hexane, **TFA** - Trifluoroacetic acid, **TEA** - Triethylamine, **THF** - Tetrahydrofuran, **TMSCl** - Trimethylsilyl chloride, **PBS** - Phosphate-buffered saline.

Synthetic schemes and experimental procedures

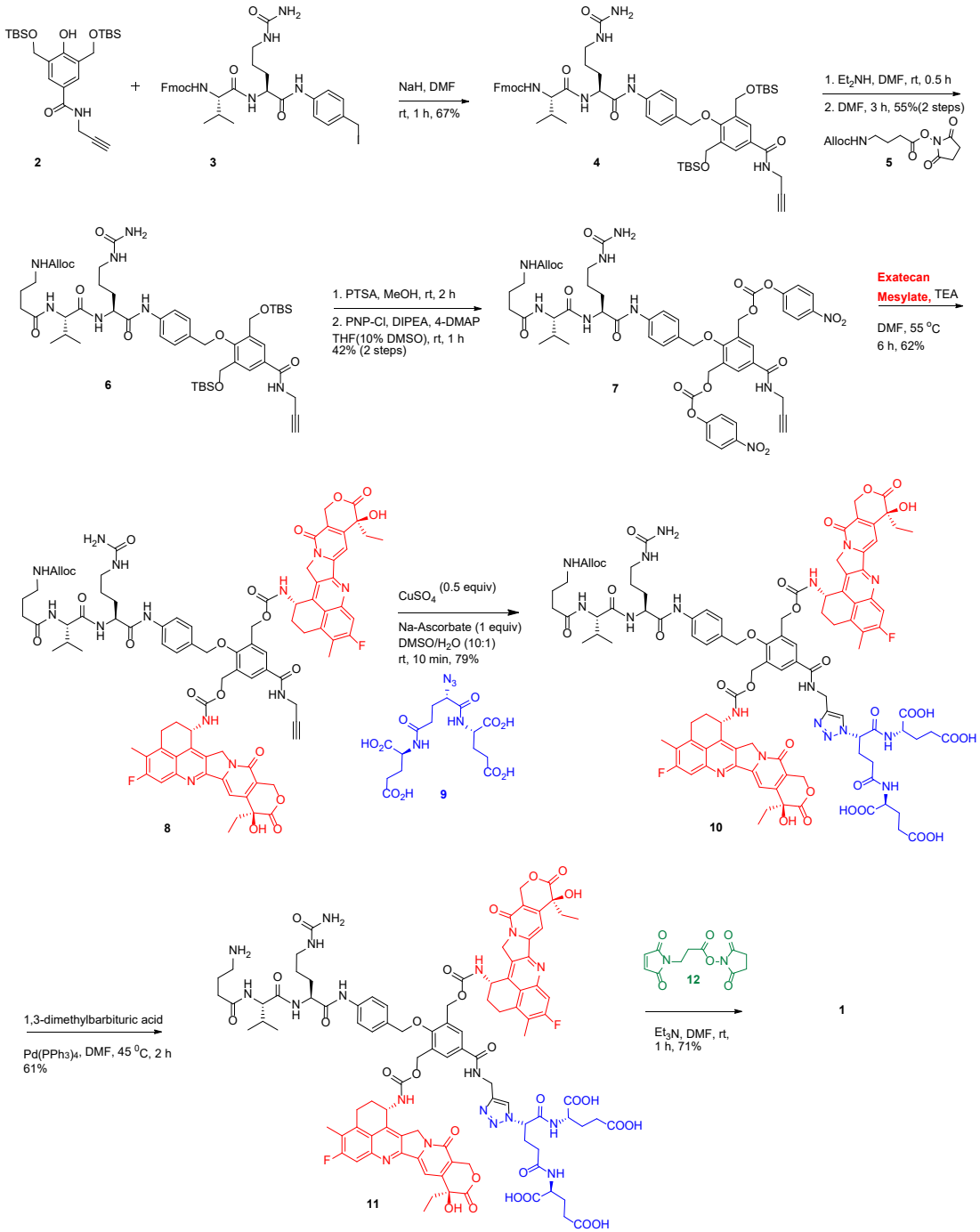

Figure S1. Synthesis of prodrug 1. The synthesis of exatecan self-immolative dimeric Prodrug 1 was achieved as presented. Phenol 2 was alkylated with iodide 3 to generate ether 4. The Fmoc protecting group of Compound **4** was then removed to give the corresponding amine, which was further reacted with NHS ester 5 to produce amide 6. The TBS protecting groups of Compound **6** were removed and the obtained di-hydroxy-benzylalcohol was activated with 4-nitrophenyl chloroformate to form di-4-nitrophenyl carbonate 7. The latter was reacted with two equivalents of exatecan to

give Compound **8**. The acetylene functionality of Compound **8** was clicked with azide 9 to produce triazole 10. Finally, the Alloc protecting group of Compound **10** was removed and the obtained amine was reacted NHS ester of maleimide-carboxylic acid to furnish Prodrug 1.

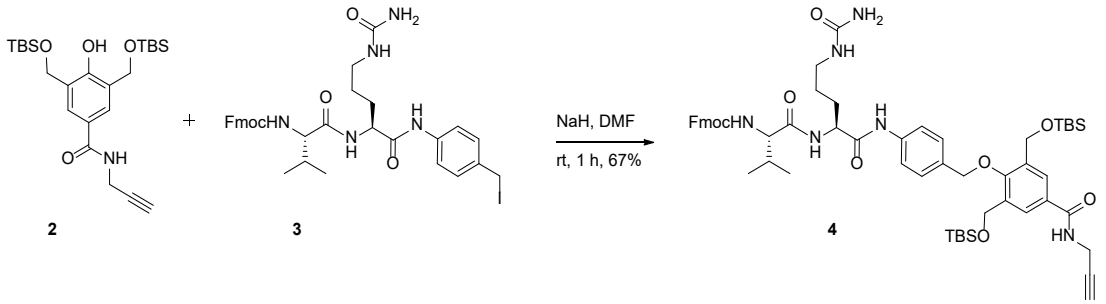

Figure S2. Synthesis of Compound 4. Compound **2** [31, 39, 40] (1.0 g, 2.16 mmol) was dissolved in dry DMF (5 mL) under argon atmosphere and cooled to 0°C. Sodium hydride (91 mg, 2.27 mmol, 60% dispersion in mineral oil) was added and the reaction was allowed to warm to RT. After stirring for 15 min at RT, Compound **3** [41] (1.54 g, 2.16 mmol) was added and the reaction was monitored by TLC (MeOH:EtOAc 10:90). Upon completion, the reaction was diluted with EtOAc (30 mL) and NH_4Cl (10 mL). The biphasic mixture was then extracted with EtOAc (3 x 30 mL), washed with brine (30 mL), dried over Na_2SO_4 and evaporated under reduced pressure. The crude product was purified by column chromatography on silica gel to afford the titled Compound **4** as an off-white solid (1.61 g, 67%). ^{1}H NMR (400 MHz, DMSO) δ 10.09 (s, 1H), 8.85 (s, 1H), 8.12 (d, *J* = 6.4 Hz, 1H), 8.01 – 7.54 (m, 6H), 7.37 (m, 6H), 5.97 (s, 1H), 5.40 (s, 2H), 4.89 (s, 2H), 4.64 (s, 4H), 4.44 (d, *J* = 4.0 Hz, 1H), 4.40 – 4.15 (m, 4H), 4.04 (s, 2H), 3.94 (d, *J* = 6.7 Hz, 2H), 3.09 – 2.91 (m, 3H), 2.87 (s, 2H), 1.99 (d, *J* = 5.5 Hz, 1H), 1.78 – 1.53 (m, 2H), 1.49 – 1.28 (m, 2H), 0.86 (s, 28H), 0.04 (s, 12H). MS (ES+) *m/z* calculated for $C_{57}H_{78}N_6O_9Si_2$: 1046.5, found 1047.9 for $[M+H]^+$.

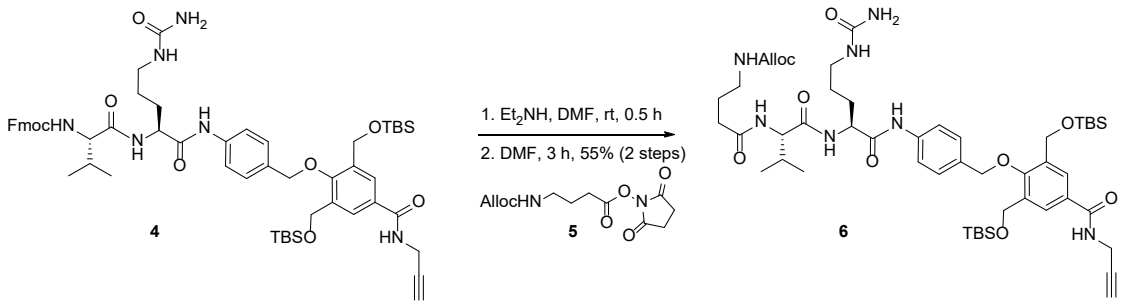

Figure S3. Synthesis of Compound 6. Compound **4** (1.2 g, 1.15 mmol) was dissolved in DMF (6 mL) and diethylamine (2 mL) was added. The reaction was monitored by TLC. Upon disappearance of starting material, the solvent and diethylamine were removed under reduced pressure. The product was dried under vacuum and directly taken for the next reaction. The crude material was dissolved in DMF (5 mL), and Compound **5** (327 mg, 1.15 mmol) was added. The mixture was stirred at RT for 2 h and the reaction was monitored by TLC. Upon completion, the solvent was removed under reduced pressure. The crude product was purified by column chromatography on silica gel to afford the titled Compound **6** as an off-white solid (630 mg, 55% over 2 steps). ^{1}H NMR (400 MHz, MeOD) δ 7.86 (s, 1H), 7.66 (d, *J* = 8.0 Hz, 2H), 7.48 (d, *J* = 8.0 Hz, 1H), 7.34 (d, *J* = 8.3 Hz, 2H), 7.10 (d, *J* = 8.3 Hz, 1H), 6.00 – 5.85 (m, 1H), 5.29 (d, *J* = 17.2 Hz, 1H), 5.17 (d, *J* = 10.3 Hz, 1H), 4.98 (s, 2H), 4.85 (s, 2H), 4.79 (s, 1H), 4.70 (s, 2H), 4.57 – 4.48 (m, 3H), 4.21 – 4.12 (m, 2H), 3.26 – 3.06 (m, 4H), 2.39 – 2.29 (m, 2H), 2.15 – 2.05 (m, 1H), 1.87 – 1.72 (m, 4H), 1.69 – 1.53 (m, 2H), 1.05 – 0.96 (m, 6H), 0.92 (s, 18H), 0.09 (s, 9H). MS (ES+) *m/z* calculated for $C_{50}H_{79}N_7O_{10}Si_2$: 993.5, found 1016.9 for $[M+Na]^+$.

A.

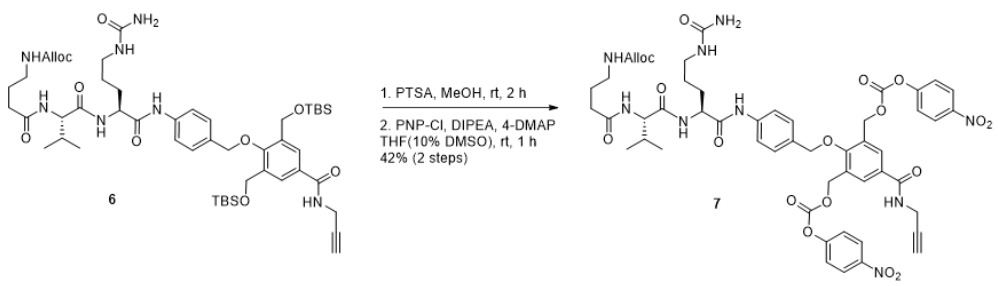

B.

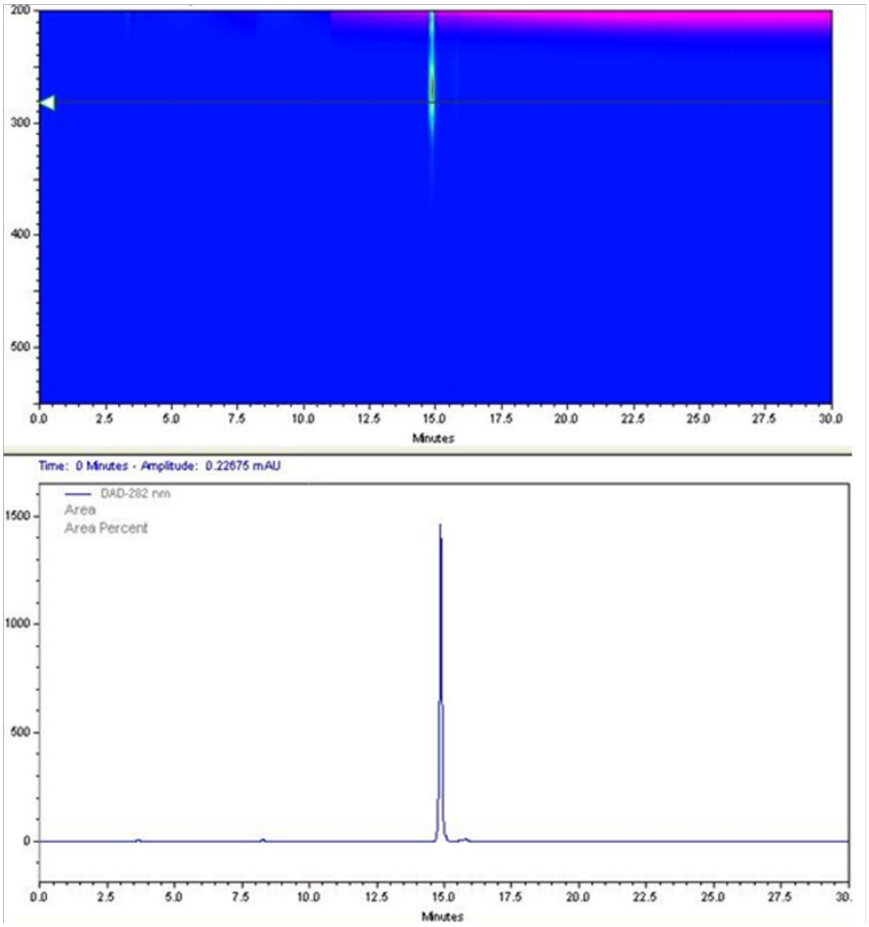

Figure S4. Synthesis and RP-HPLC chromatograms of Compound 7. (A) Compound **6** (625 mg, 0.63 mmol) was dissolved in MeOH (4 mL) and 4-touenesulfonic acid monohydrate (PTSA, 12 mg, 0.063 mmol) was added. The reaction was monitored by TLC. Upon completion the reaction mixture was diluted with EtOAc (20 mL) and saturated $NaHCO_3$ (5 mL) was added. The biphasic mixture was then extracted with EtOAc (3 x 20 mL), washed with brine (20 mL), dried over Na_2SO_4, and evaporated under reduced pressure. The crude product was dissolved in dry THF/DMSO solvent system (8 mL, THF: DMSO 10:1) before DIPEA (0.45 mL, 2.52 mmol) and 4-DMAP (4 mg, 0.03 mmol) were added. The mixture was cooled to 0°C. 4-Nitrophenyl chloroformate (PNP-Cl, 317 mg, 1.58 mmol) was then added portion wise and the reaction was stirred for 1 h at RT. The progress of the reaction was monitored by TLC.

Upon completion, the solution was directly loaded on silica gel and the product was purified by column chromatography to afford Compound **7** as off-white solid (289 mg, 42% over 2 steps). MS (ES+) *m/z* calculated for $C_{52}H_{57}N_9O_{18}$: 1095.4, found 1096.7 for $[M+H]^+$. Analytical RP-HPLC: Column C18 5µ, 250x4.6 mm. Eluent: ACN/H_2O (H_2O with 0.1% of TFA). Method: 30-100 % ACN gradient. t_R for Compound **7**: 15.0 min. **(B)** HPLC elution gradient ACN and water with 0.1 TFA (30-100%).

A.

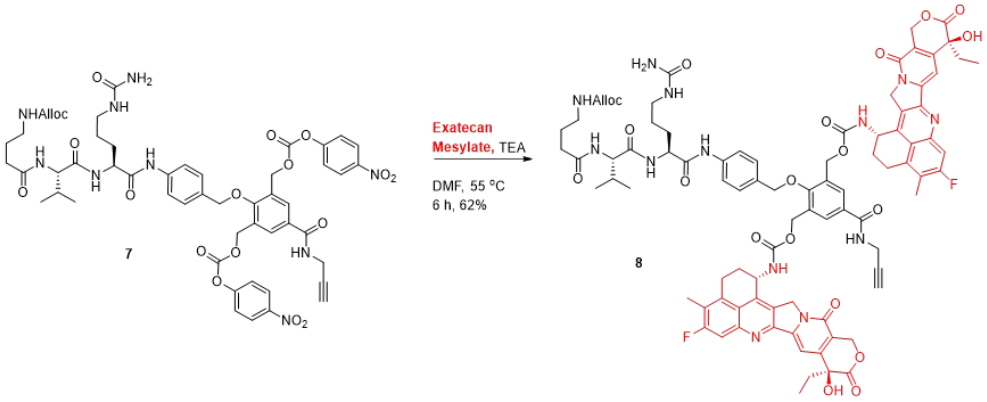

B.

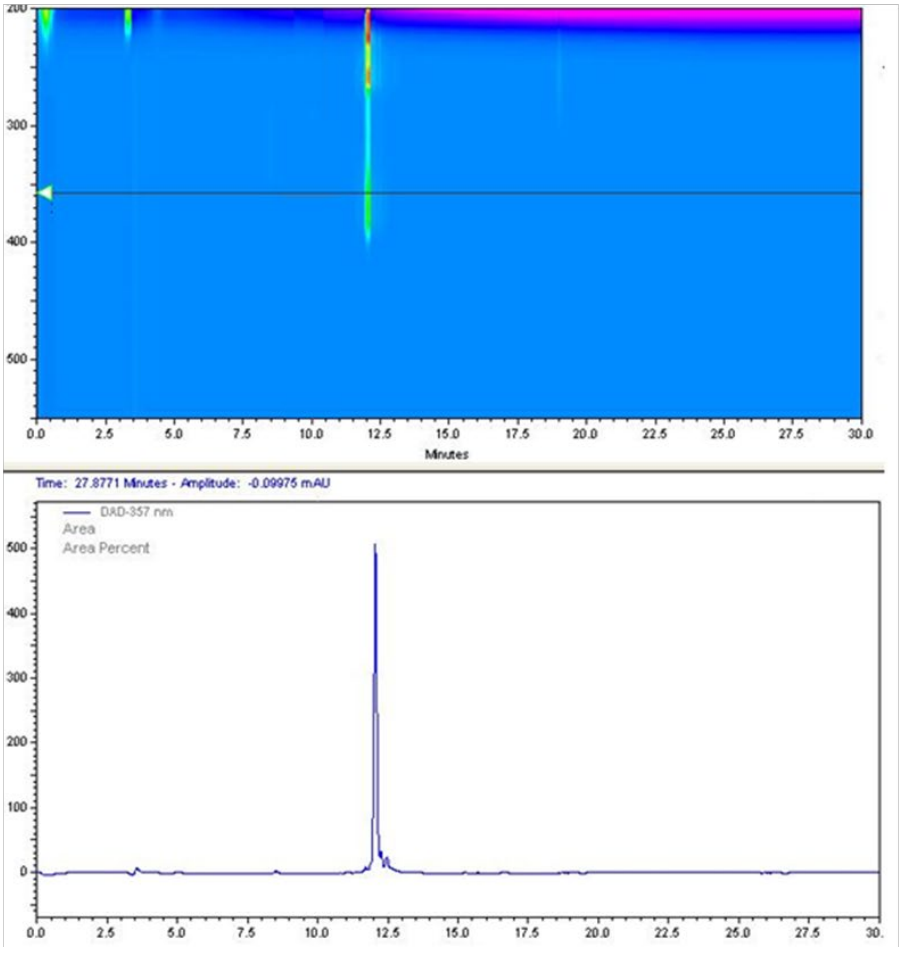

Figure S5. Synthesis and RP-HPLC chromatograms of Compound 8. (A) Compound **7** (80 mg, 0.07 mmol) was dissolved in dry DMF (2 mL) at RT. Exatecan Mesylate (77 mg, 0.14 mmol) was added followed by Et_3N (60 μL, 0.44 mmol. The reaction mixture was stirred at 55^{o}C for 6 h and the progress of the reaction was monitored by RP-HPLC. Upon completion the product was isolated by reverse phase preparative HPLC (30-100% ACN in water with 0.1% TFA, 20 min) to afford Compound **8** as yellow solid (76 mg, 62%). MS (ES+) *m*/*z* calculated for $C_{88}H_{91}F_2N_{13}O_{20}$: 1687.6, found 845.7 for $[M/2+2H]^+$. Analytical RP-HPLC: Column C18 5µ, 250x4.6 mm. Eluent: ACN/H_2O (H_2O with 0.1% of TFA). Method: 30-100% ACN gradient. t_R for Compound **8**: 12.4 min. **(B)** HPLC elution gradient ACN and water with 0.1 TFA (30-100%).

A.

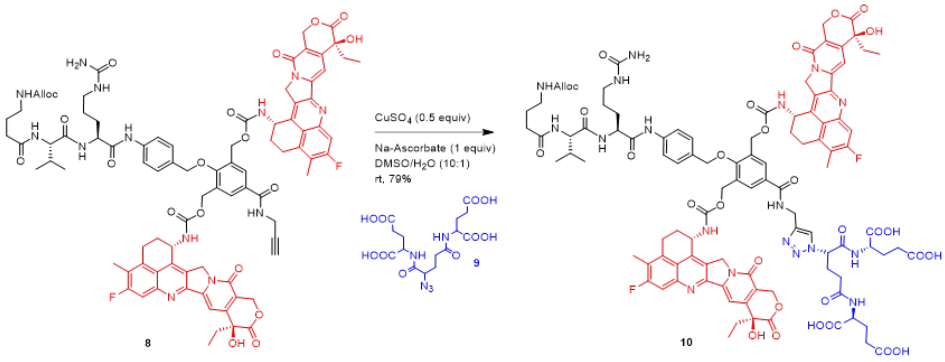

B.

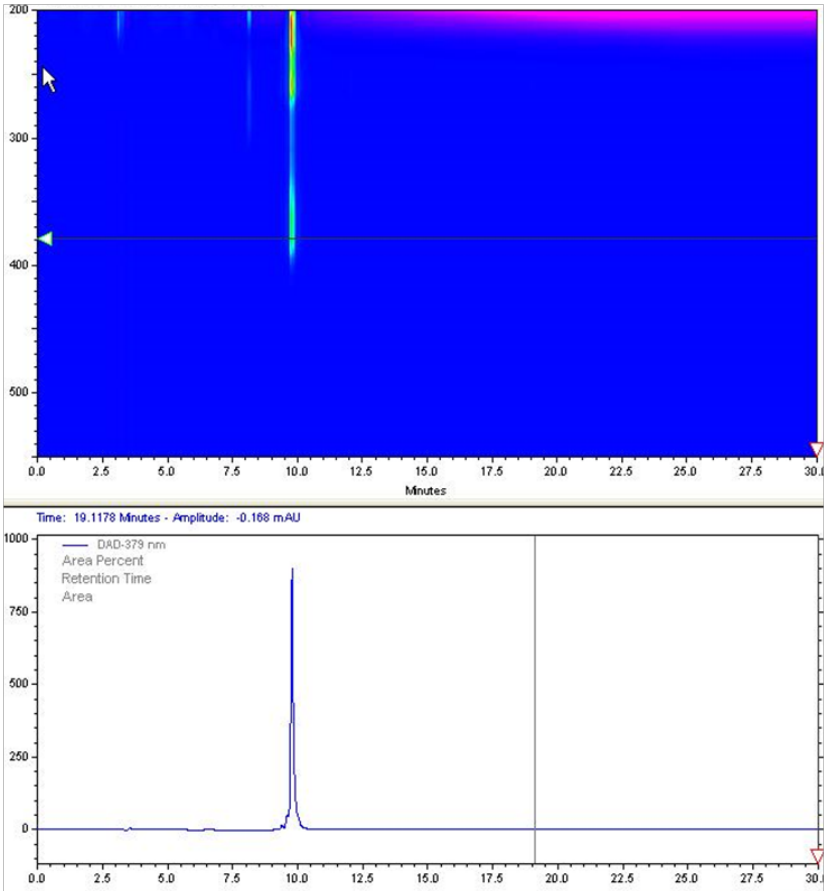

Figure S6. Synthesis and RP-HPLC chromatograms of Compound 10. (A) Compound **8** (65 mg, 0.04 mmol) and azide **9** (86 mg, 0.2 mmol) was dissolved in a solvent system DMSO/H_2O (10:1, 2 mL) followed by the addition of $CuSO_4.5H_2O$ (5 mg, 0.02 mmol) and sodium ascorbate (3.2 mg, 0.03 mmol). The solution was degassed with argon for 30 min and then stirred at RT. After 30 min of stirring the progress of the reaction was monitored by RP-HPLC. Upon completion the product was isolated by reverse phase preparative HPLC (30-100% ACN in water with 0.1% TFA, 20 min) to afford Compound **10** as yellow solid (64 mg, 79%). MS (ES+) *m/z* calculated for $C_{103}H_{112}F_2N_{18}O_{30}$: 2119.9, found 1061.4 for $[M/2+H]^+$. Analytical RP-HPLC: Column C18 5µ, 250x4.6 mm. Eluent: ACN/H_2O (H_2O with 0.1% of TFA). Method: 30-100% ACN gradient. t_R for Compound **10**: 10.07 min. **(B)** HPLC elution gradient ACN and water with 0.1 TFA (30-100%).

A.

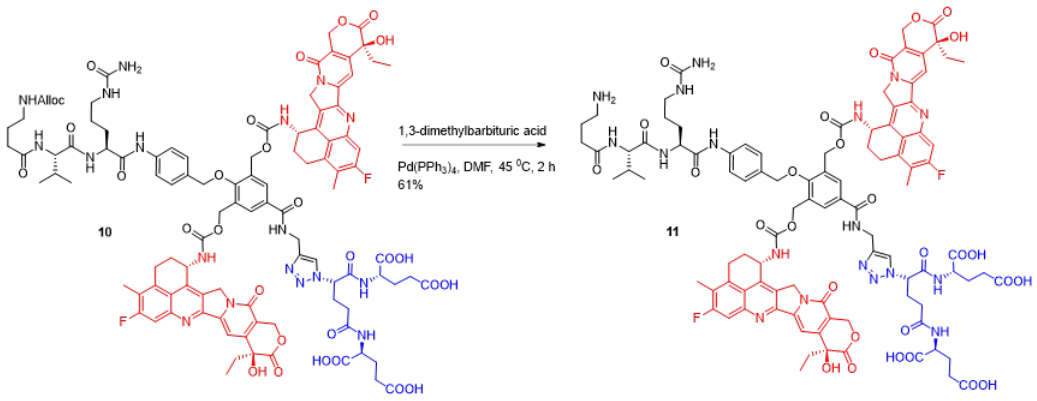

B.

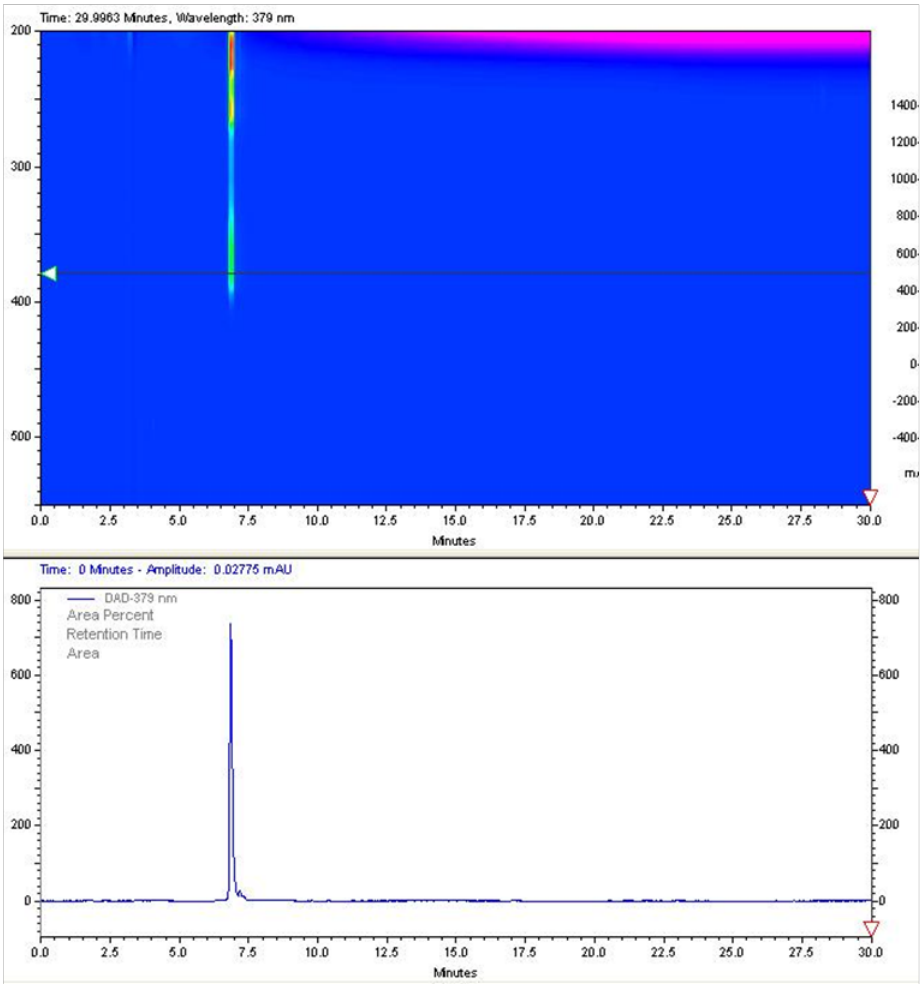

Figure S7. Synthesis and RP-HPLC chromatograms of Compound 11. (A) Compound **10** (52 mg, 0.025 mmol) was dissolved in DMF (2 mL) under argon followed by the addition of $Pd(PPh_3)_4$ (15 mg, 0.012) and 1,3-dimethyl barbituric acid (8.0 mg, 0.05 mmol). The mixture was stirred at 45°C under argon and the progress of the reaction was monitored by RP-HPLC. After 30 min the HPLC chromatogram shows that about 50% conversion has occurred. Thereby another batch of $Pd(PPh_3)_4$ and 1,3-dimethyl barbituric acid were added. Upon completion of the reaction after 2 h the product was isolated by reverse phase preparative HPLC (10-90% ACN in water with 0.1% TFA, 20 min) to afford Compound **11** as a yellow solid (30 mg, 61%). MS (ES+) *m/z* calculated

for $C_{99}H_{108}F_2N_{18}O_{28}$: 2035.7, found 1019.2 for $[M/2+H]^+$. Analytical RP-HPLC: Column C18 5µ, 250x4.6 mm. Eluent: ACN/H_2O (H_2O with 0.1% of TFA). Method: 30-100 % ACN gradient. t_R for Compound **11**: 6.5 min. **(B)** HPLC elution gradient ACN and water with 0.1 TFA (30-100%).

A.

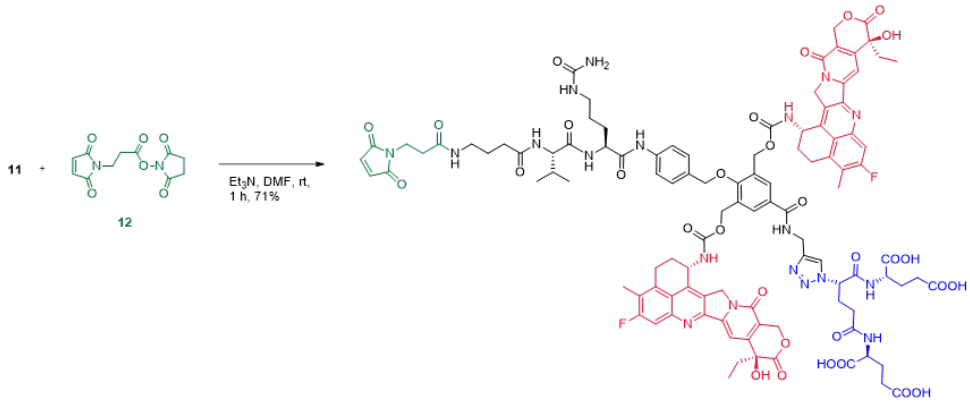

B.

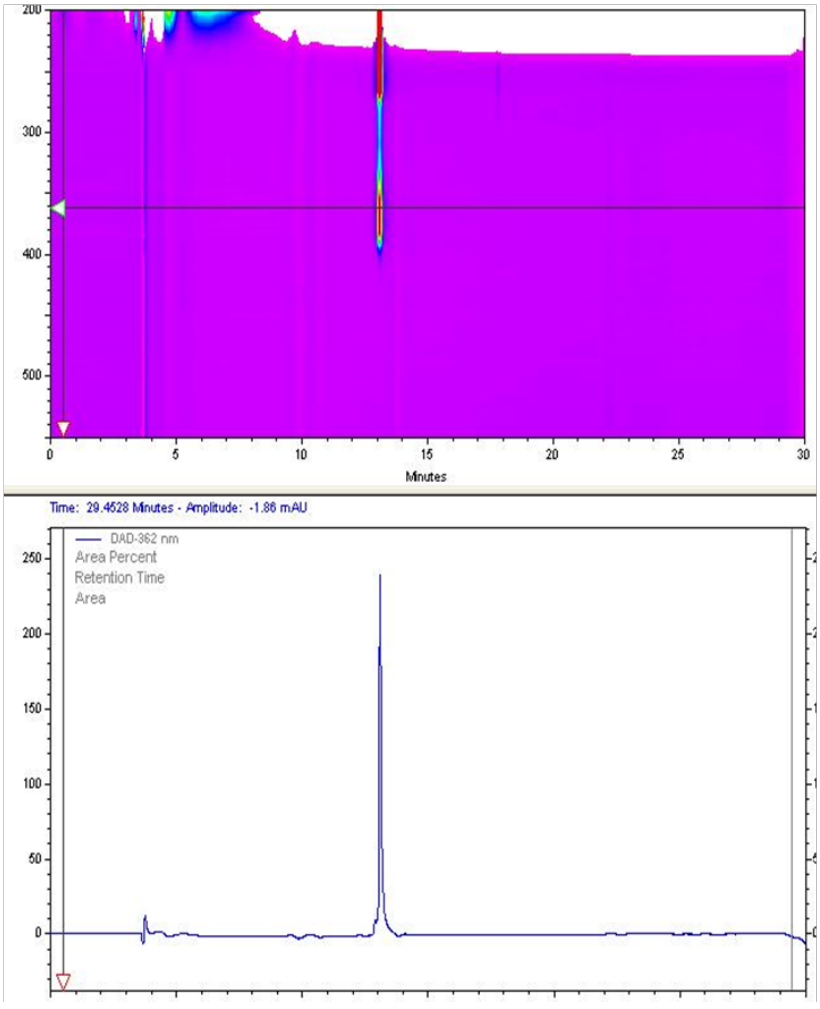

Figure S8. Synthesis and RP-HPLC chromatograms of Prodrug 1. (A) Compound **11** (25 mg, 0.012 mmol) and Compound **12** (4 mg, 0.014 mmol) were dissolved in dry DMF (1.5 mL). Et_3N was added and the reaction mixture was stirred at RT for 1 h. Upon

completion, as monitored by RP-HPLC, the product was purified by reverse phase preparative HPLC (10-90% ACN in water with 0.1% TFA, 20 min) to afford the final Prodrug **1** as yellow solid (19 mg, 71%). MS (ES+) *m/z* calculated for $C_{106}H_{113}F_2N_{19}O_{31}$: 2186.79, found 1094.6 for $[M/2+H]^+$. Analytical RP-HPLC: Column C18 5µ, 250x4.6 mm. Eluent: ACN/H_2O (H_2O with 0.1% of TFA). Method: 10-90 % ACN gradient. t_R for Prodrug **1**: 13.2 min.

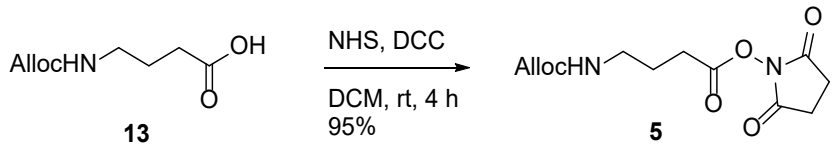

Figure S9. Synthesis of Compound 5. Compound **13** [42] (750 mg, 4.0 mmol) was dissolved in DCM (8 mL) and cooled to 0°C. N-hydroxysuccinimide (692 mg, 6.0 mmol) was added followed by N,N'-Dicyclohexylcarbodiimide (908 mg, 4.4 mmol). The reaction was allowed to warm up to RT and stirring continued for 4 h. Upon completion the turbid mixture was filtered, washed with DCM. The combined organic solution was concentrated, and the product was purified by silica gel column chromatography to afford Compound **4** (1.08 g, 95%) as white solid. ^{1}H NMR (400 MHz, $CDCl_3$) δ 5.89 (ddt, *J* = 16.2, 10.7, 5.5 Hz, 1H), 5.28 (dd, *J* = 17.2, 1.2 Hz, 1H), 5.18 (d, *J* = 10.4 Hz, 1H), 4.53 (d, *J* = 4.8 Hz, 2H), 3.27 (q, *J* = 6.4 Hz, 2H), 2.82 (s, 4H), 2.66 (dd, *J* = 13.2, 5.9 Hz, 2H), 1.95 (p, *J* = 6.9 Hz, 2H). ^{13}C NMR (101 MHz, $CDCl_3$) δ 169.33, 168.40, 156.51, 132.97, 117.73, 65.66, 39.82, 28.36, 25.67, 25.02. MS (ES+) *m/z* calculated for $C_{12}H_{16}N_2O_6$:284.1, found 285.3 for $[M+H]^+$.

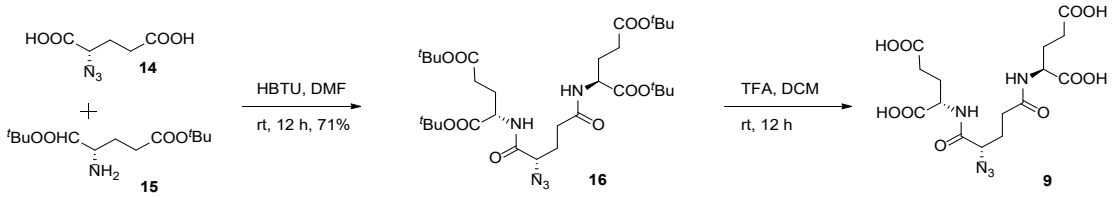

Figure S10. Synthesis of Compound 9.

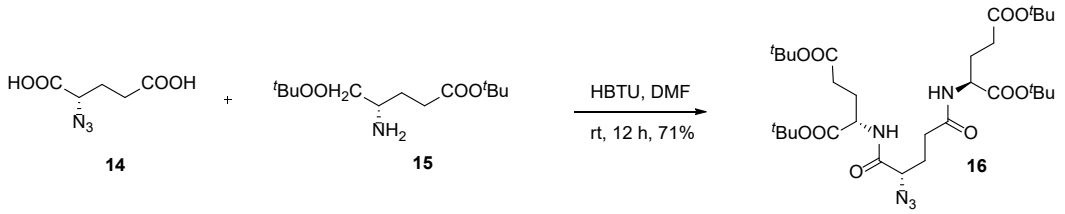

676

677 **Figure S11. Synthesis of Compound 16.** Compound **16** is prepared according to the
678 literature procedure[43]. The L-azidoglutamic acid **14**[44] (222 mg, 1.3 mmol) was
679 dissolved in dry DMF (10 mL) under an argon atmosphere. HBTU (1.23 g, 3.25 mmol)
680 was added to the solution and the mixture was stirred for 5 min at RT. DIPEA (2.30 mL,
681 13.0 mmol) was added to the solution in a single portion, followed immediately by L-
682 glutamic acid ditertiary butyl ester **15** (760 mg, 2.6 mmol). The reaction mixture was
683 stirred overnight, after which the solvent was removed in vacuum. The crude product
684 was purified by silica gel column chromatography to afford Compound **16** (597 mg,
685 71% with respect to **14**) as gummy liquid. ^{1}H NMR (400 MHz, $CDCl_3$) δ 8.17 (d, *J* = 8.7
686 Hz, 1H), 7.83 (d, *J* = 8.7 Hz, 1H), 4.59 (td, *J* = 9.6, 4.3 Hz, 1H), 4.49 (td, *J* = 9.5, 4.3 Hz,
687 1H), 3.40 (dd, *J* = 11.4, 4.2 Hz, 1H), 2.45 – 2.23 (m, 6H), 2.14 (dt, *J* = 18.2, 6.2 Hz, 4H),
688 1.91 – 1.72 (m, 2H), 1.44 (m, *J* = 13.5, 3.3 Hz, 36H). ^{13}C NMR (101 MHz, $CDCl_3$) δ 174.36,
689 173.78, 172.52, 171.60, 170.54, 83.58, 83.53, 80.97, 80.89, 59.98, 52.50, 52.38, 32.11,
690 31.93, 31.78, 28.18, 28.12, 28.09, 27.79, 26.86, 26.71. MS (ES+) *m/z* calculated for
691 $C_{31}H_{53}N_5O_{10}$: 655.4, found 656.7 for $[M+H]^+$.

692

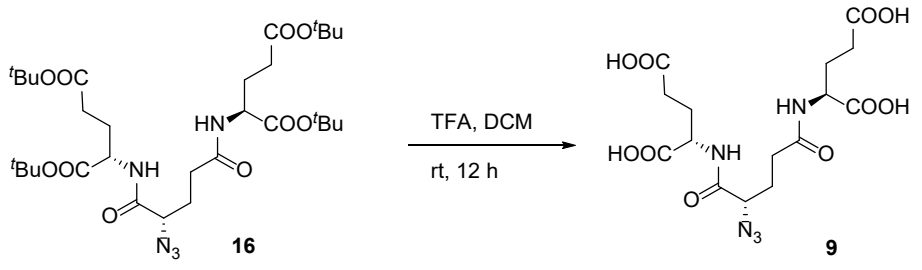

693

694 **Figure S12. Compound 9.** Compound **16** (550 mg, mmol) was dissolved in DCM (3 mL)
695 and TFA (3 mL) was added. The reaction was stirred overnight. Upon completion, as
696 monitored by TLC, the solvent and TFA were removed under reduced pressure. The
697 product formation was confirmed by MS and the crude material was directly taken for
698 the click reaction. MS (ES+) *m/z* calculated for $C_{15}H_{21}N_5O_{10}$: 431.1, found 432.3 for
699 $[M+H]^+$.

700

NMR and MS Spectra

A.

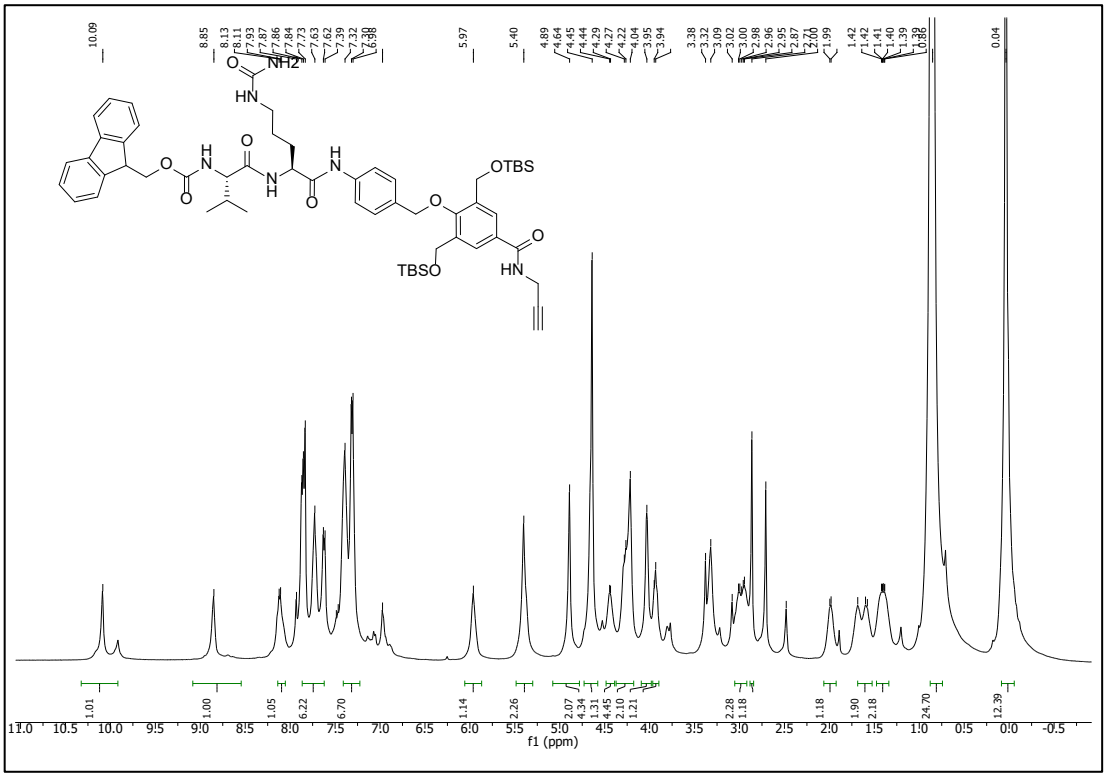

B.

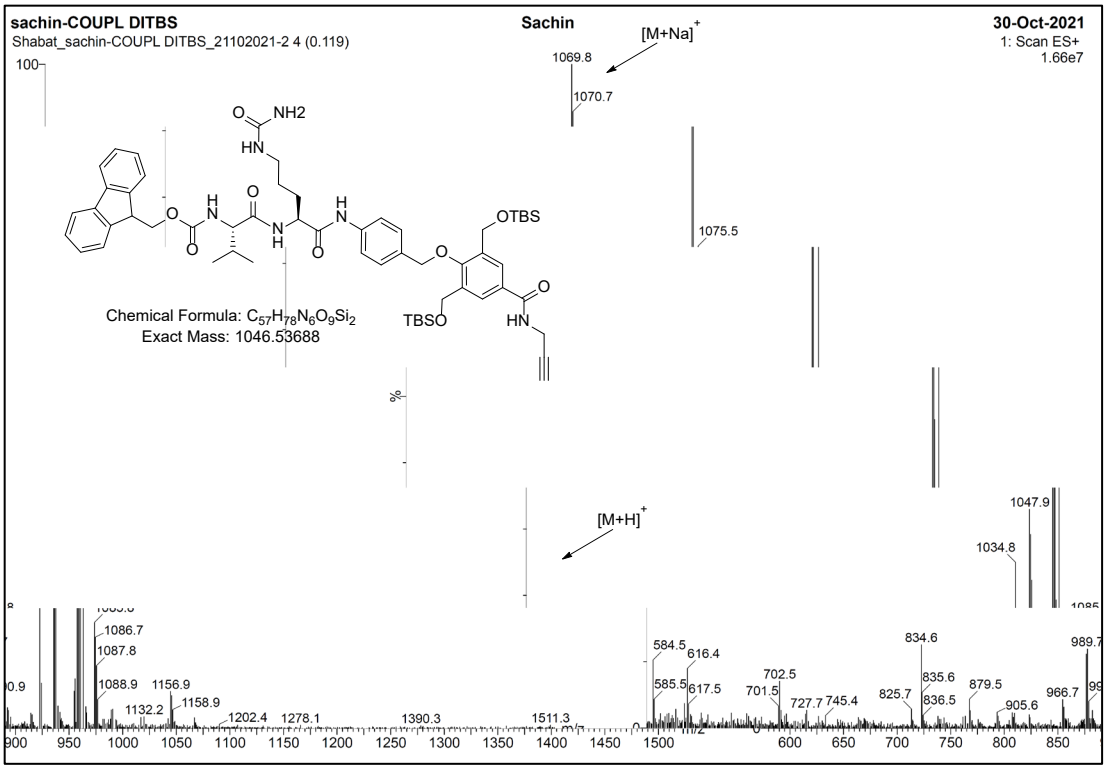

Figure S13. (A) ^{1}H-NMR spectra of Compound **4. (B)** MS of Compound **4.**

A.

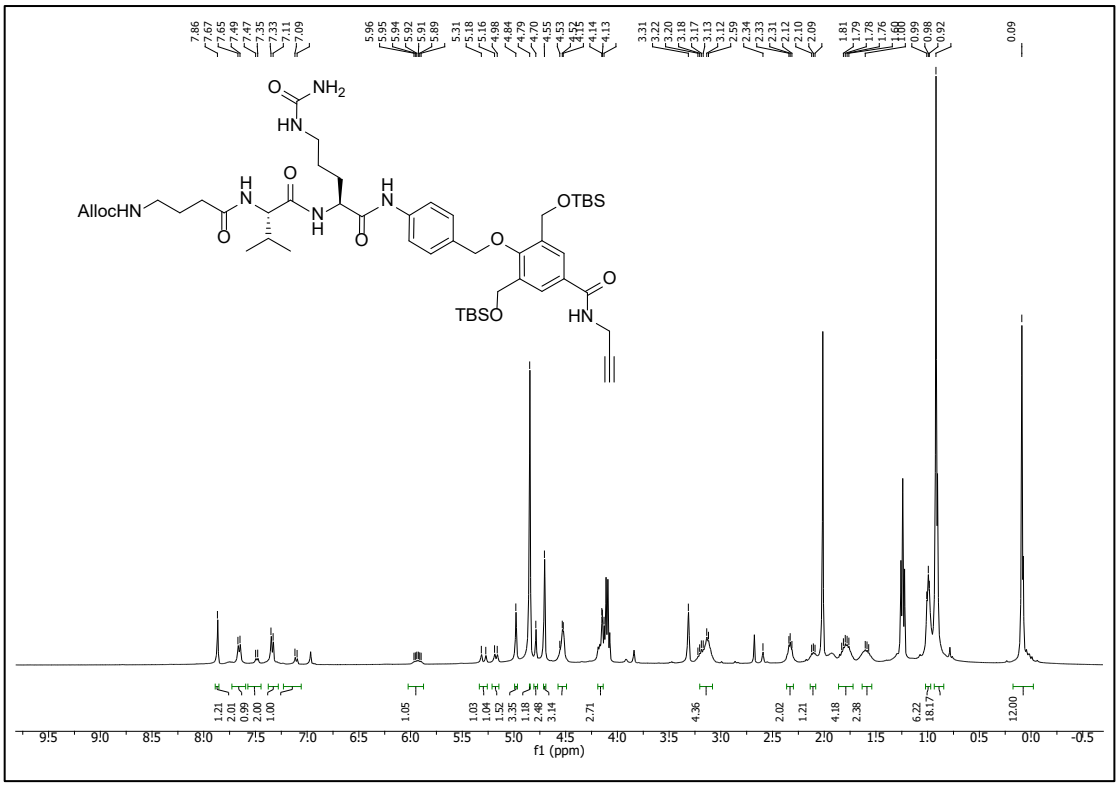

B.

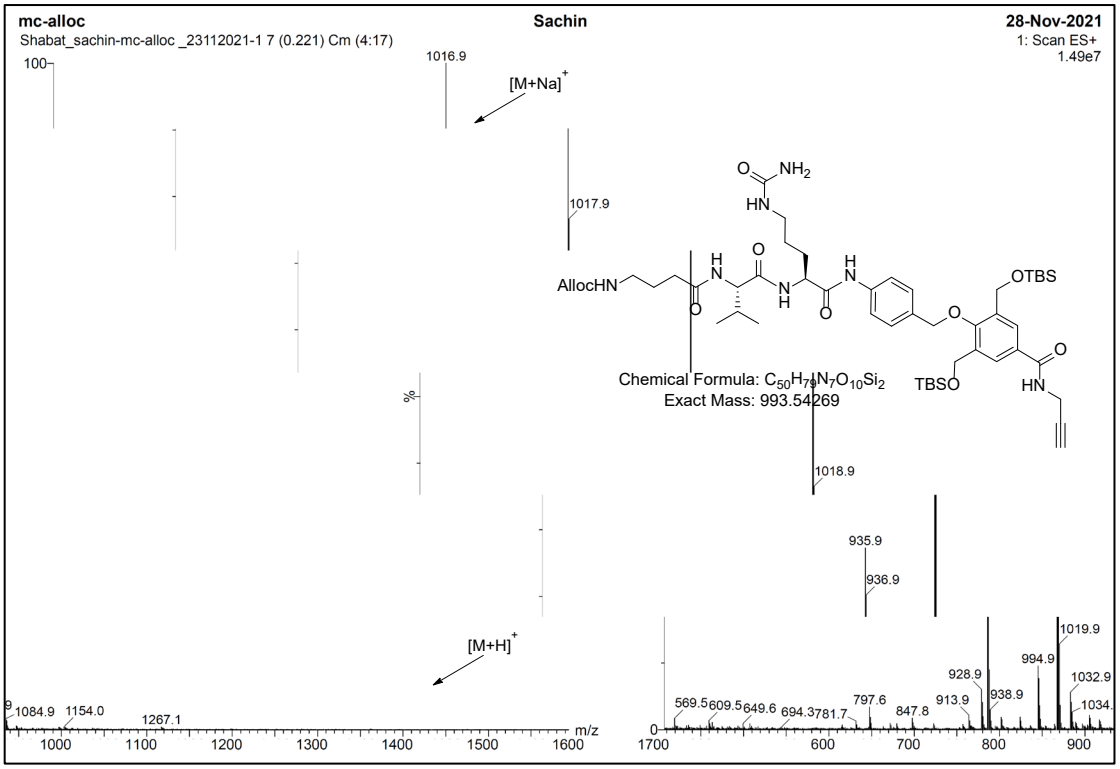

Figure S14. (A) ^{1}H-NMR spectra of Compound **6. (B)** MS of Compound **6.**

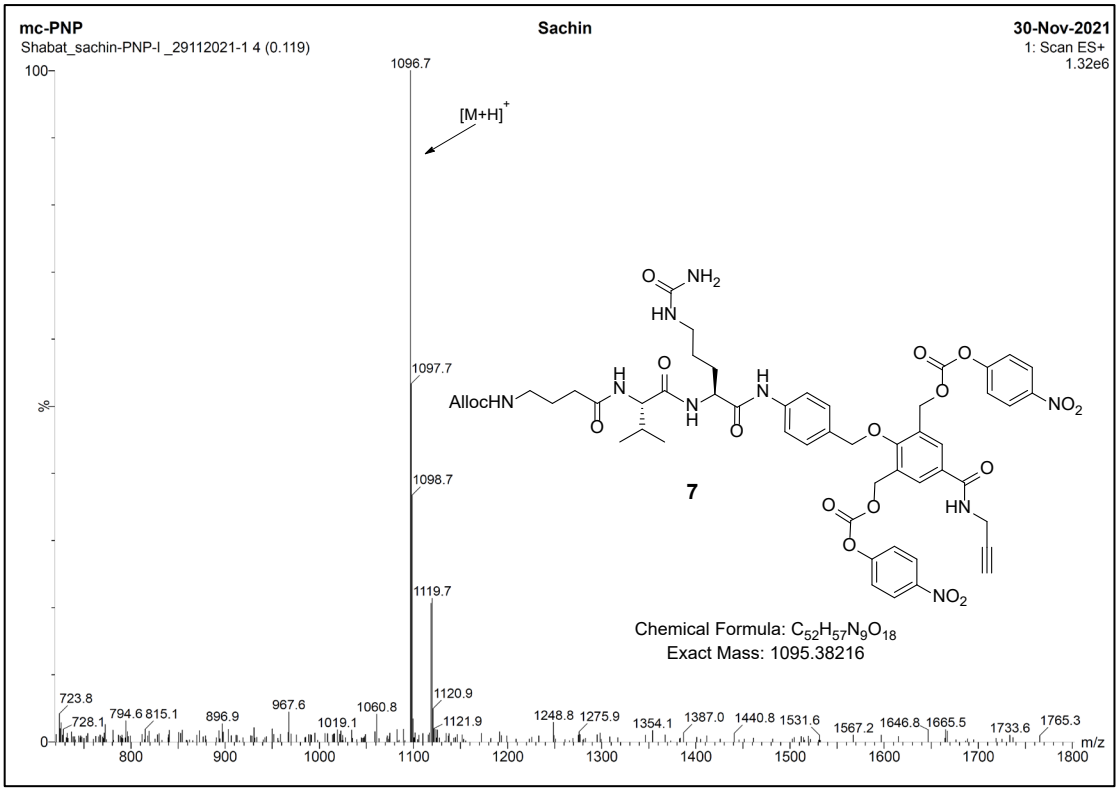

712

713 **Figure S15.** MS of Compound **7**

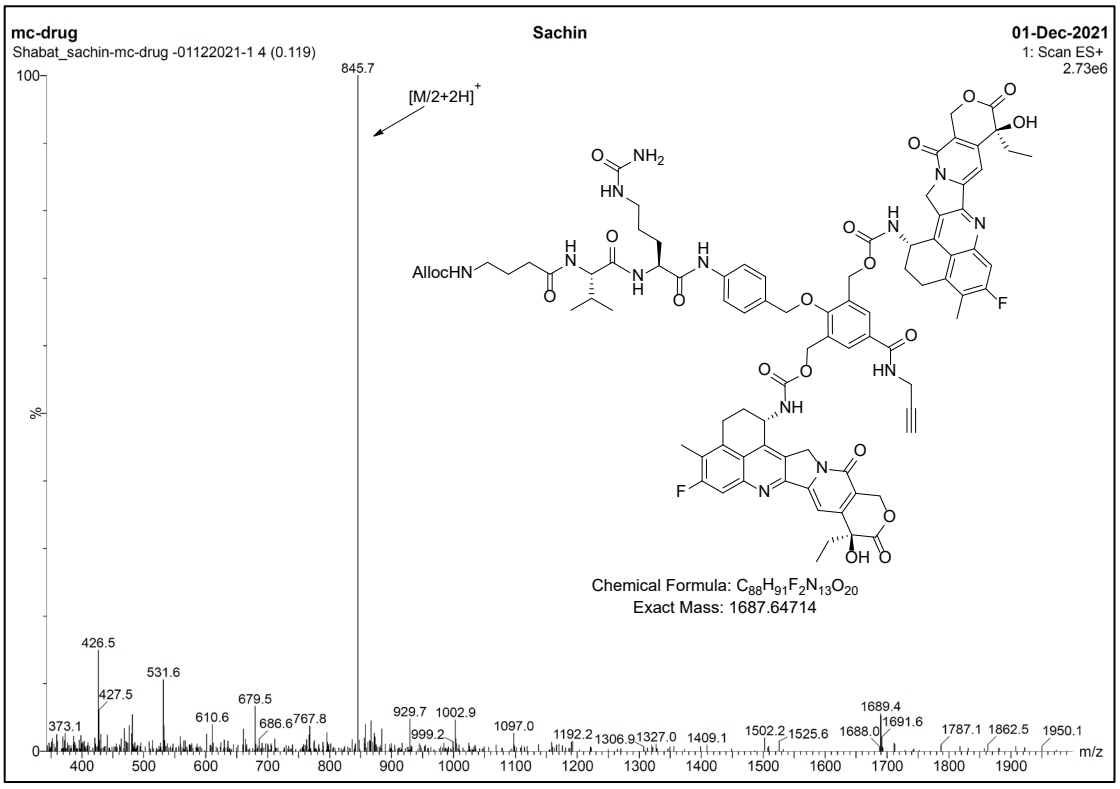

714

715 **Figure S16.** MS of Compound **8**

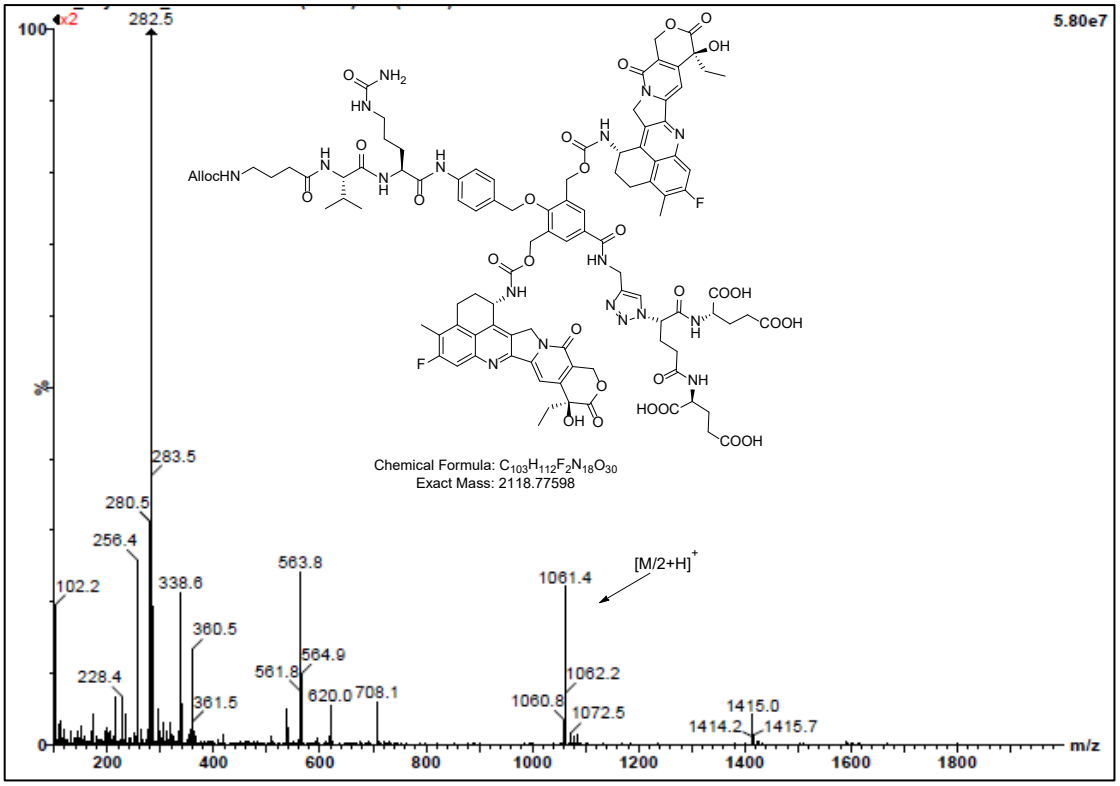

716

717 **Figure S17.** MS of Compound **10**

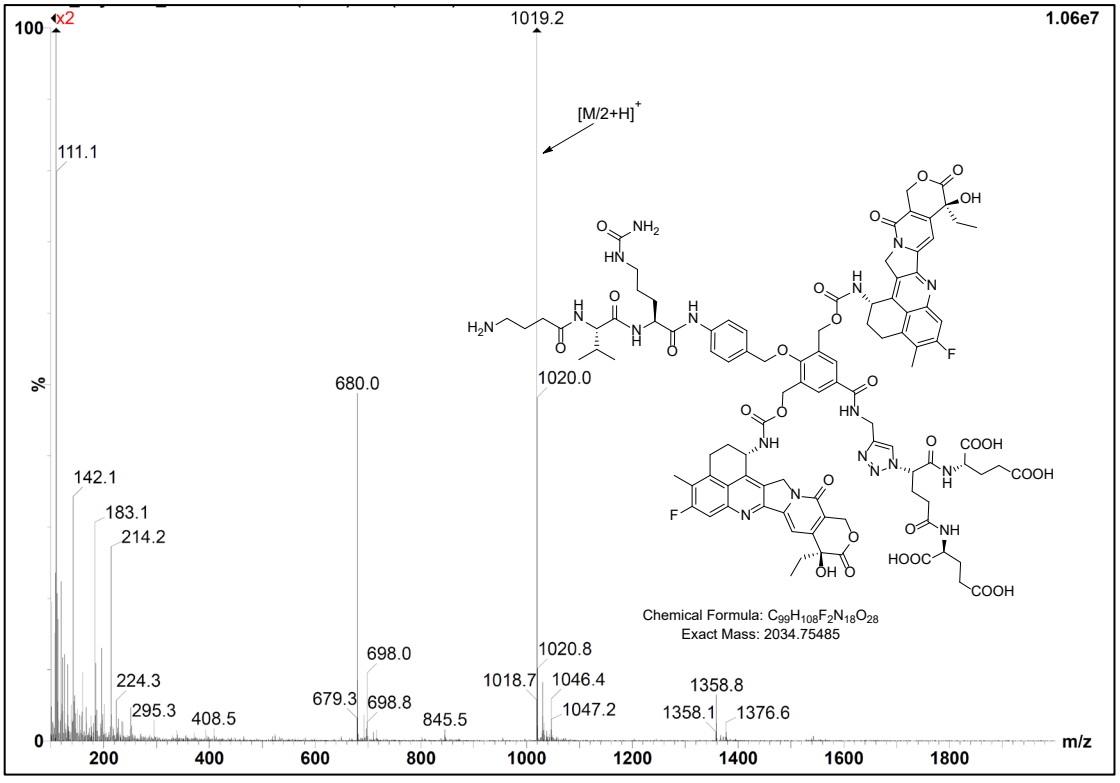

718

719 **Figure S18.** MS of Compound **11**

720

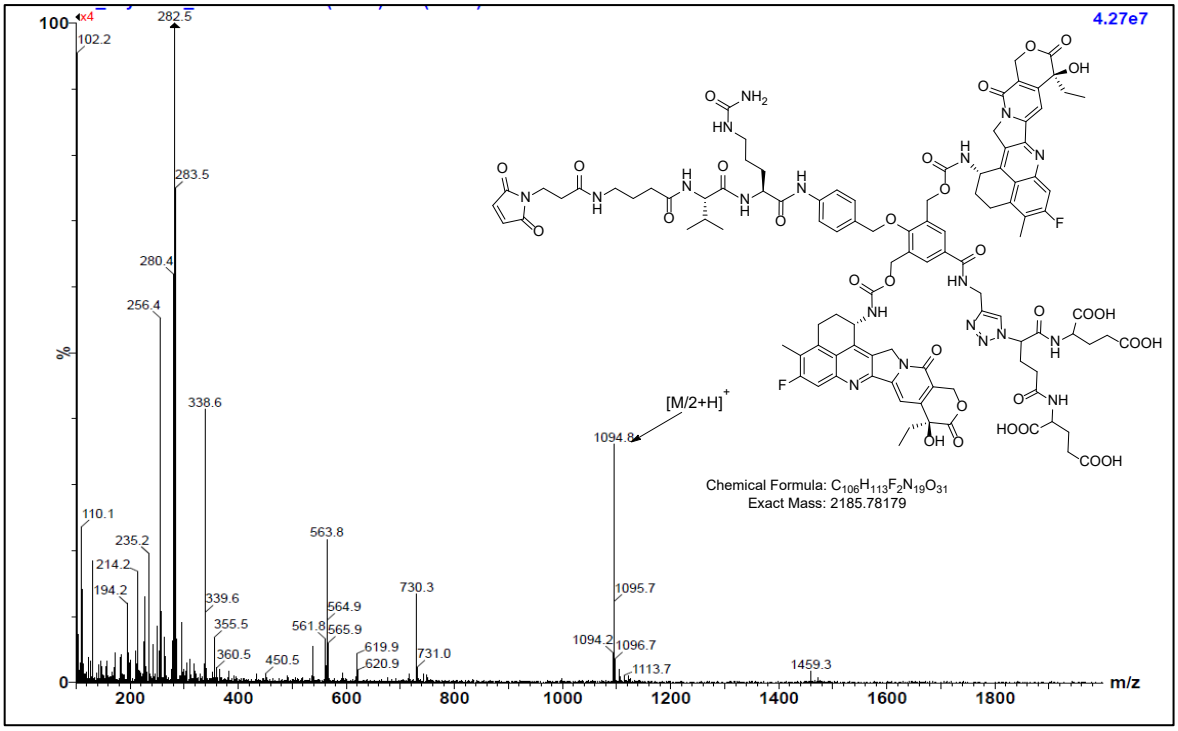

721 **Figure S19.** MS of Prodrug **1**

722

723

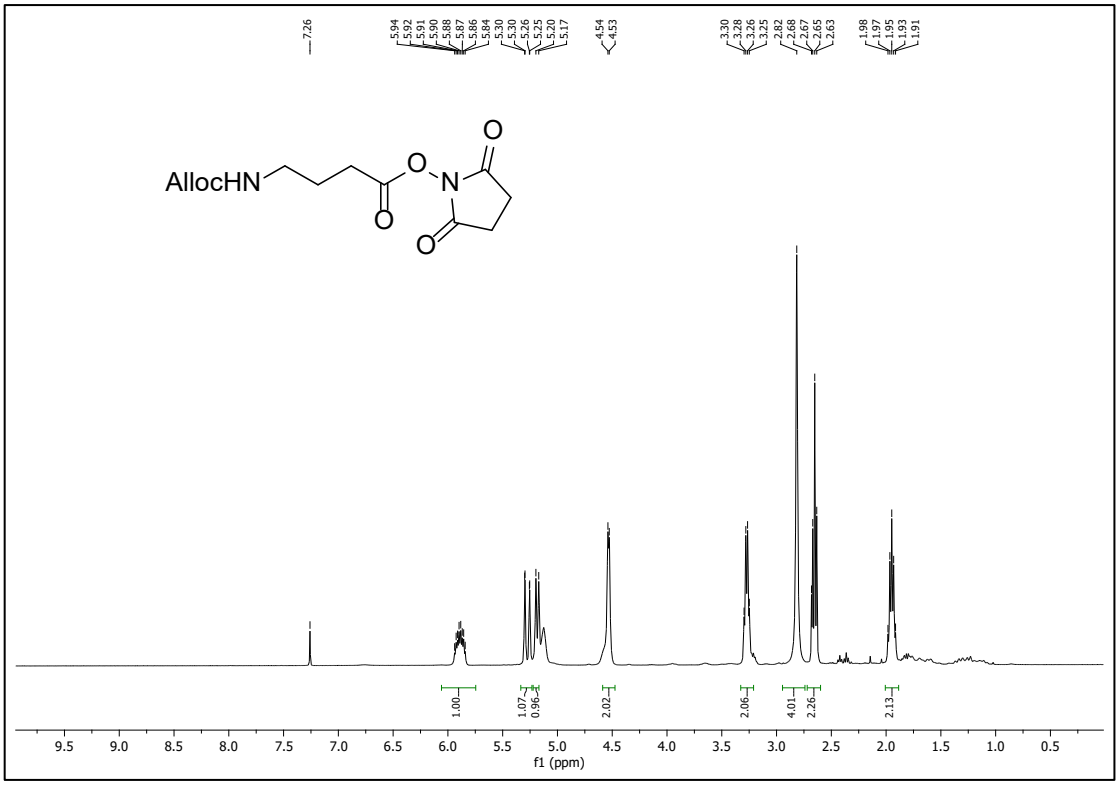

724

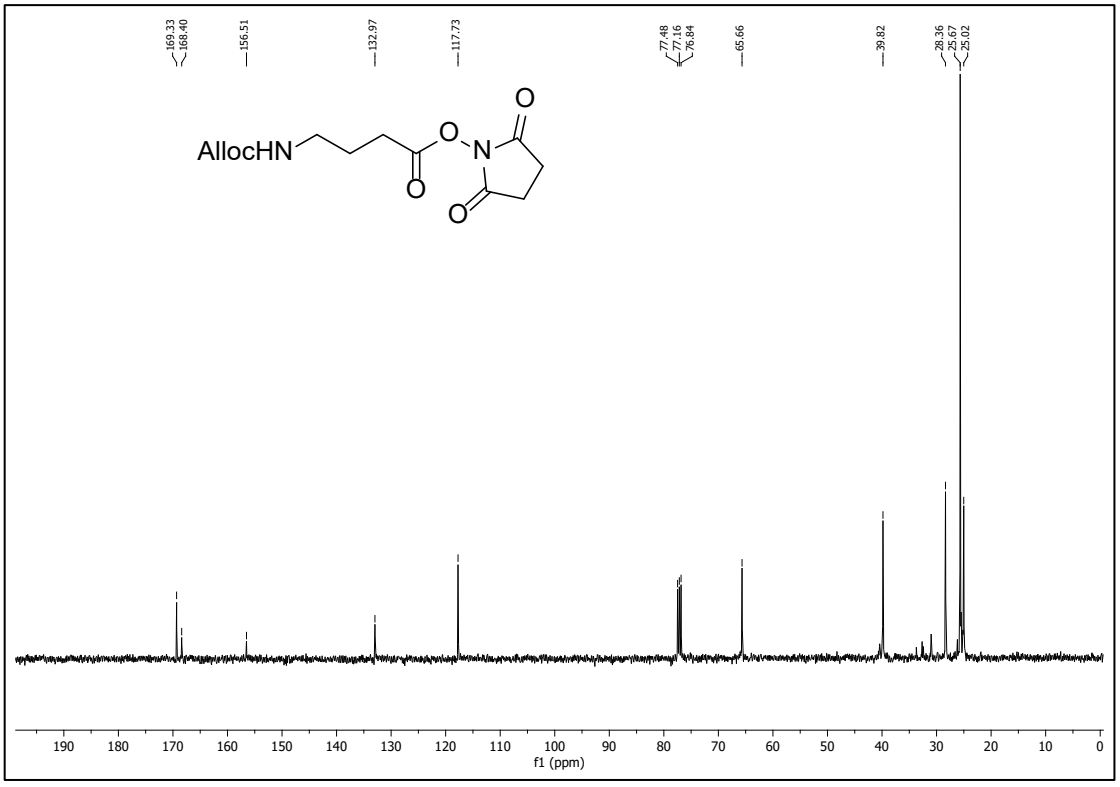

725 **Figure S20.** ^{1}H-NMR and ^{13}C-NMR spectra of Compound **5**

726

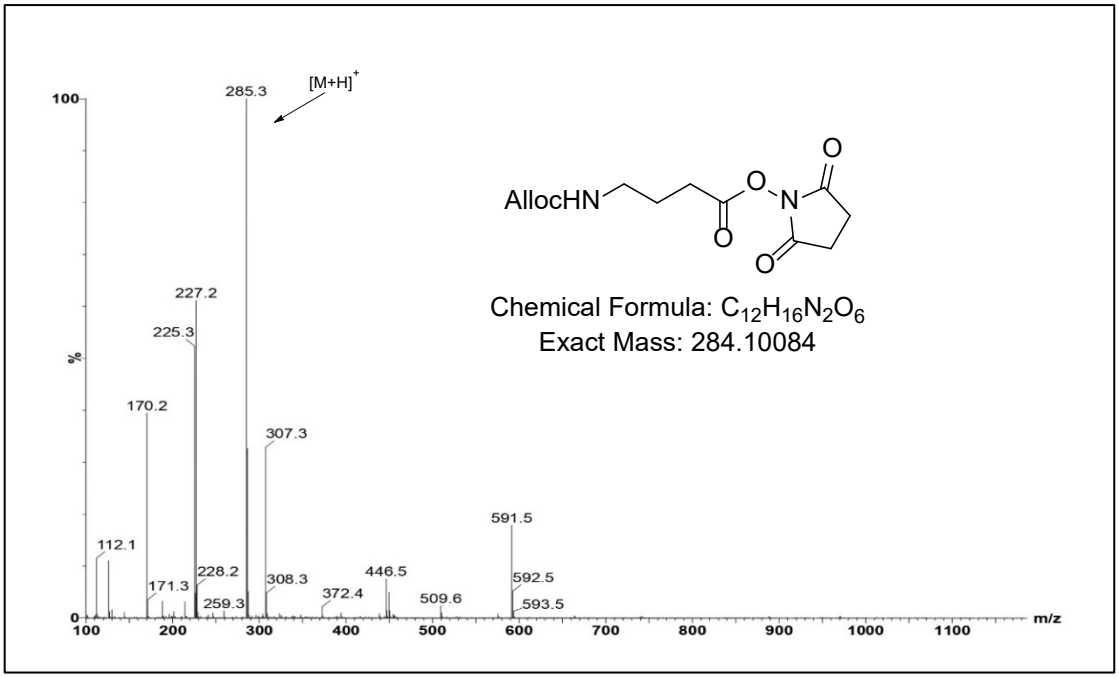

727

728 **Figure S21.** MS of compound **5**

729

730

731

732

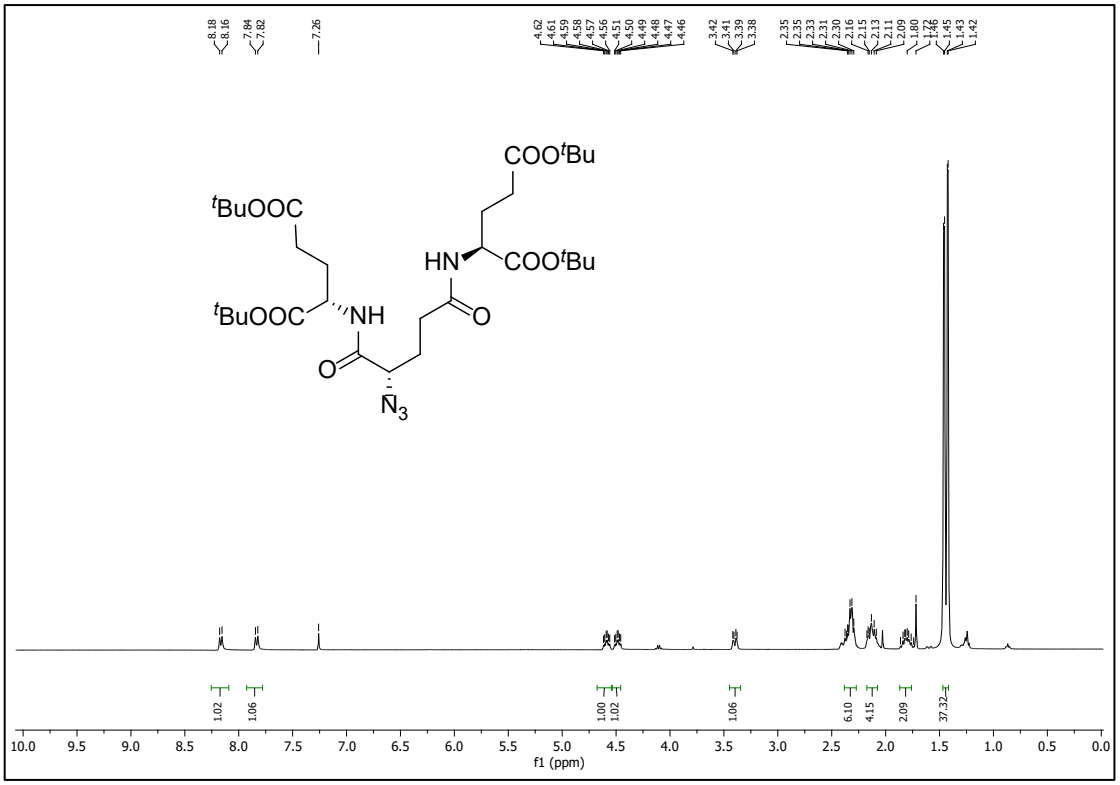

733

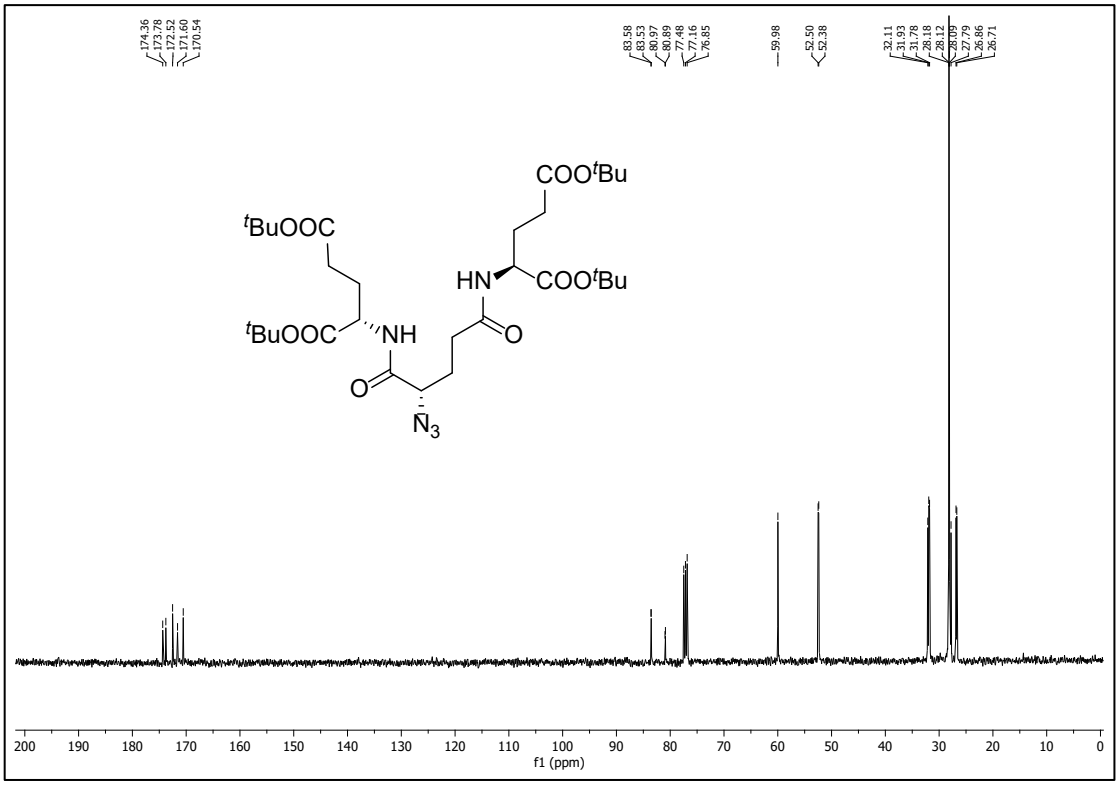

734 **Figure S22.** ^{1}H-NMR and ^{13}C-NMR spectra of Compound **16**

735

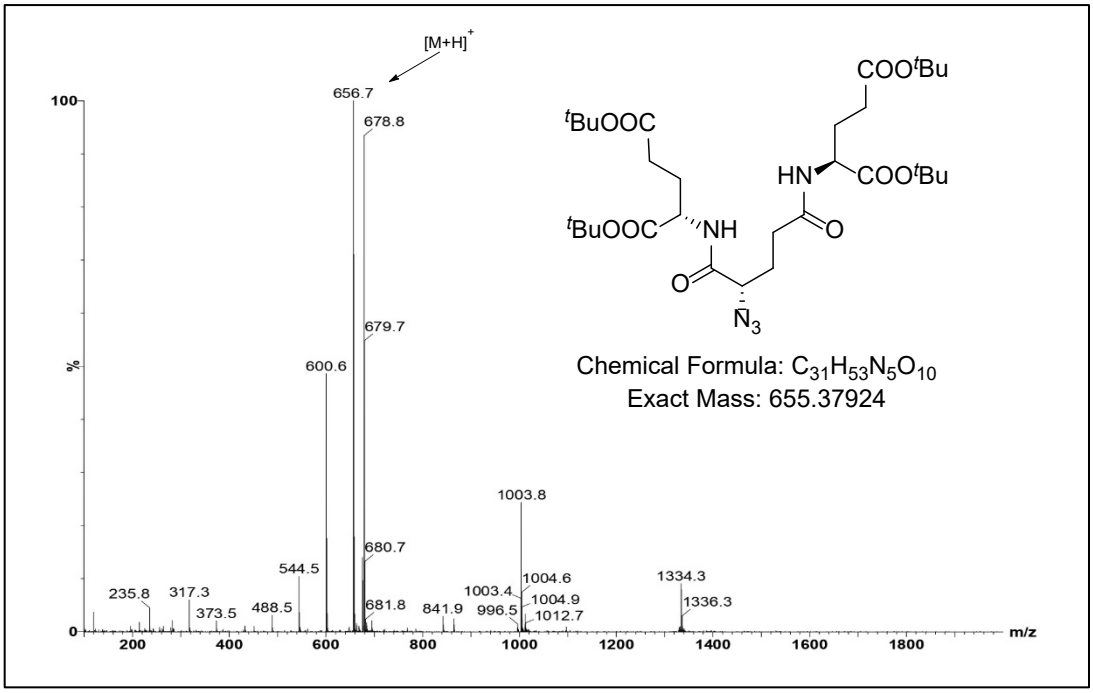

736

737 **Figure S23.** MS of Compound **16**

738

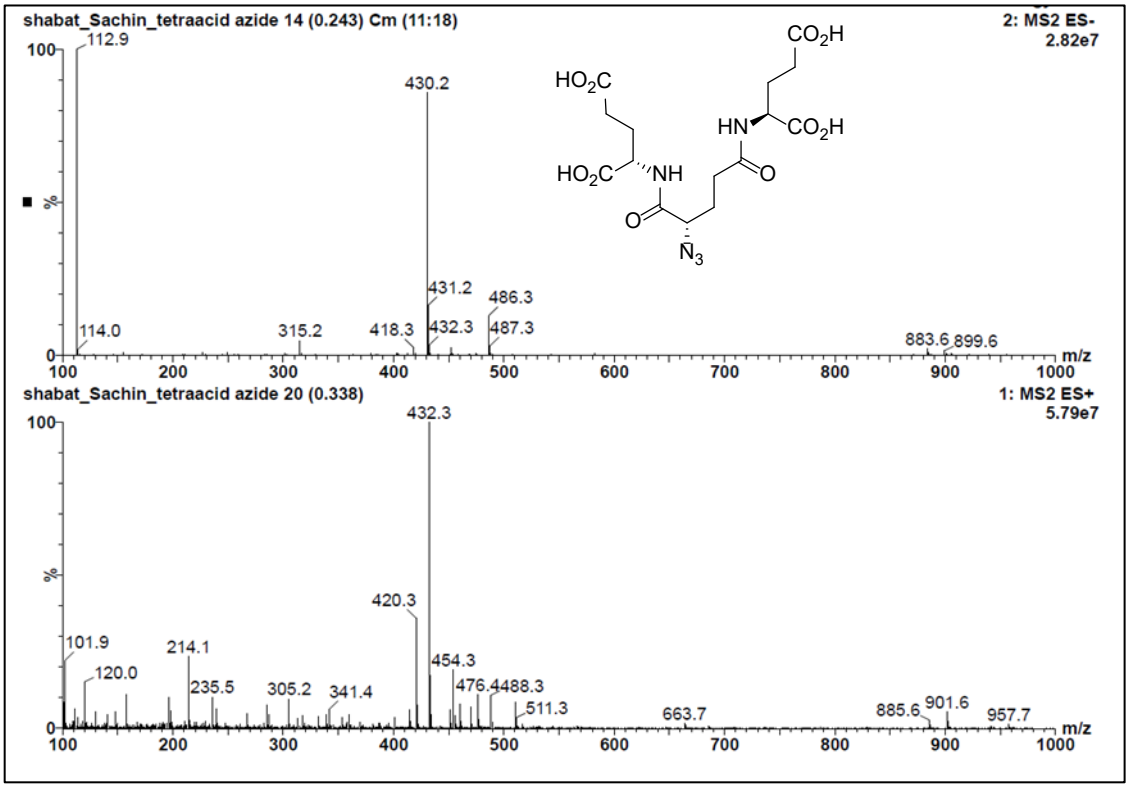

739

740 **Figure S24.** MS of Compound **9**

741

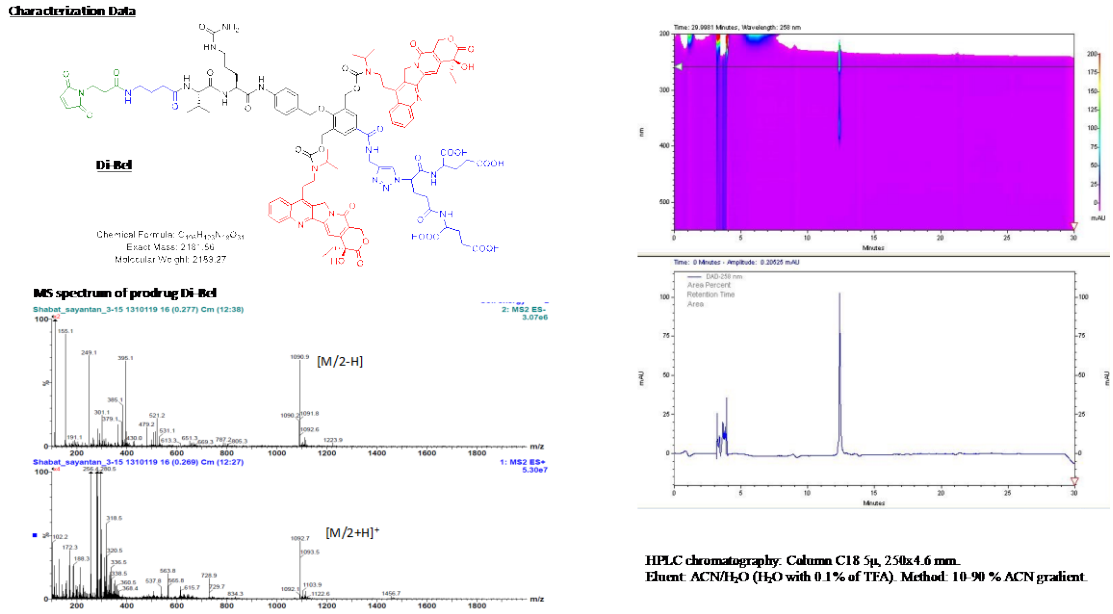

742

743 **Figure S25. Belotecan dimeric prodrug 2 synthesis.** Belotecan dimeric prodrug was
744 synthesized in a similar manner to the procedures described above for the exatecan
745 dimeric prodrug.

746

747

748 **DXd prodrug 3 synthesis**

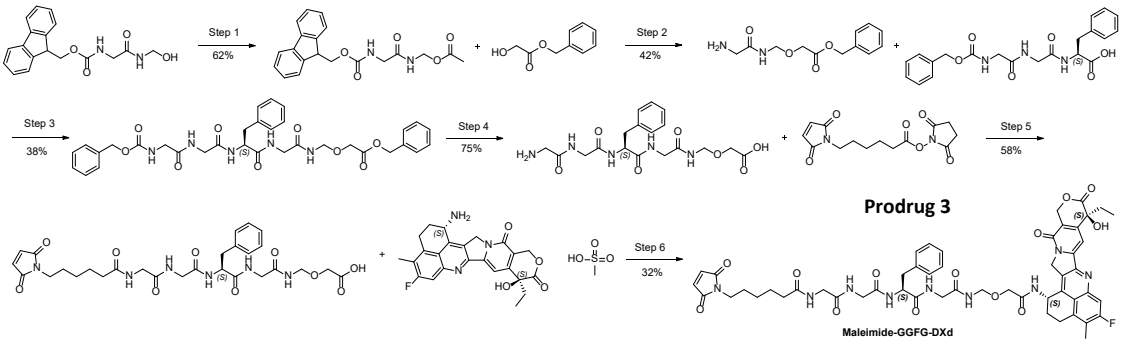

749

750 **Figure S26. DXd prodrug 3 synthesis.** Experimental procedures are described below**.**

751

752 **DXd prodrug 3 synthesis – Experimental procedures**

753 **Step 1:**

754 To a stirred solution of [2-(9H-Fluoren-9-ylmethoxycarbonylamino)-acetylamino]-
755 acetic acid (25.00 g; 69.84 mmol; 1.00 eq.) in THF (500.00 ml; 20.00 V) and Toluene

(150.00 ml; 6.00 V) (3:1) ratio was added Pyridine (6.83 ml; 83.81 mmol; 1.20 eq.) and followed by triacetoxyplumbyl acetate (37.54 g; 83.81 mmol; 1.20 eq.) at RT and heated to reflux for 5 h at 80°C.

After that, the reaction solution was cooled to RT, the insoluble material was removed by filtration through Celite bed, and the filtrate was concentrated under reduced pressure. The obtained residue was dissolved in ethyl acetate, washed with water and saturated brine and then the organic layer was dried over anhydrous sodium sulfate.

After the solvent was removed under reduced pressure, the obtained residue was purified by column chromatography using 60-120 mesh silica gel eluent at 70 to 85 % ethyl acetate in pet ether to afford Acetic acid [2-(9H-fluoren-9-ylmethoxycarbonylamino)-acetylamino]-methyl ester (16.00 g; 43.35 mmol; 62.1 %; white solid; Purified Product).

LC/MS Chromatography: Column: ATLANTIS dC18 (50x4.6mm) 5 µm; Mobile phase: A:0.1% HCOOH in H_2O:ACN(95:5) B:ACN; Flow Rate: 1.5 mL/min: [M+Na]+ = 391, RT = 2.22 minute

^{1}H NMR: 400 MHz, DMSO-d6:8.94 (t, J = Hz, 1H), 7.90 (d, J = 7.20 Hz, 2H), 7.72 (d, J = 7.20 Hz, 2H), 7.57 (t, J= Hz, 1H), 7.38 (d, J = 20.00 Hz, 2H), 7.32 (d, J = 0.80 Hz, 2H), 5.11 (d, J = Hz, 2H), 4.31-4.24 (m, 3H) 3.35 (d, J = Hz, 2H), 2.00 (s, 3H)

Step 2:

To a stirred solution of Acetic acid [2-(9H-fluoren-9-ylmethoxycarbonylamino)-acetylamino]-methyl ester (16.00 g; 43.35 mmol; 1.00 eq.) in THF (160.00 mL; 10.00 V) was added Hydroxy-acetic acid benzyl ester (14.50 g; 86.39 mmol; 1.99 eq.) followed by p-toulenesulfonic acid monohydrate (1.66 mL; 4.76 mmol; 0.11 eq.) at 0°C and stirred at same temperature for 2 h then stirred at RT for 1 h.

After completion, the reaction solution was charged with water and extracted with ethyl acetate, washed with 10% NaHCO3 solution and The obtained organic layer was dried over sodium sulfate and filtered, the filtrate was concentrated to obtain crude product The obtained residue was purified by silica gel (230-400 mesh) column chromatography eluent at 70 to 75 % EA in PE to afford benzyl 2-{[2-({[(9H-fluoren-9-

yl)methoxy]carbonyl}amino)acetamido]methoxy}acetate (9.00 g; 18.35 mmol; 42.3 %; white solid; Purified Product).

LC/MS Chromatography: Column: ATLANTIS dC18 (50x4.6 mm) 5 µm; Mobile phase: A: 0.1% HCOOH in H_2O:ACN(95:5) B: ACN; Flow Rate :1.5 mL/min: [M+Na]+ = 497, RT = 2.52 min.

^{1}H NMR: 400 MHz, DMSO-d6: 8.75 (t, J = Hz, 1H), 7.90 (d, J = 7.48 Hz, 2H), 7.81 (d, J = 65.32 Hz, 2H), 7.61 (t, J = Hz, 1H), 7.58-7.31 (m, 8H), 5.15 (s, 2H), 4.64 (d, J = 6.68 Hz, 2H), 4.30-4.21 (m, 3H), 4.18 (d, J = 17.24 Hz, 2H), 3.63 (d, J = 6.04 Hz, 2H)

Step 3:

To a stirred solution of benzyl 2-{[2-({[(9H-fluoren-9-yl)methoxy]carbonyl}amino)acetamido] methoxy} acetate (9.00 g; 18.36 mmol; 1.00 eq.) in DMF (90.00 mL; 10.00 V) was added 2,3,4,6,7,8,9,10-Octahydropyrimido[1,2-a]azepine (2.85 g; 18.36 mmol; 1.00 eq.) at 0°C and stirred at RT for 30 min, completion of the reaction was confirmed by LC-MS. The reaction mixture was directly used for the next step without further purification.

To the solution of the reaction mixture was added (2S)-2-[2-(2-{[(benzyloxy)carbonyl]amino} acetamido)acetamido]-3-phenylpropanoic acid (7.67 g; 18.36 mmol; 1.00 eq.) followed by 1-Hydroxy-pyrrolidine-2,5-dione (2.56 g; 22.03 mmol; 1.20 eq.) and (3-Dimethylamino-propyl)-ethyl-carbodiimide hydrochloride (4.27 g; 22.03 mmol; 1.20 eq.) the resulted reaction mixture was stirred at RT for 2h, to that was added 0.1N HCl solution (500 mL) and stirred for 30 min, then the product was extracted with DCM, the collected organic layer was dried over anhydrous sodium sulphate, filtered and concentrated to afford crude product.

The crude product was purified by column chromatoghraphy using 230-400 mesh silica gel, all Fmoc impurities were removed by eluting 45% to 50% EA in pet ether and the product eluent at 4 to 5 % methanol in DCM to afford impure product which was later agitated with di ethyl ether and filtered, then again agitated with ethyl acetate and filtered, dried to afford benzyl 2-({2-[(2S)-2-[2-(2-{[(benzyloxy)carbonyl]

amino}acetamido)acetamido]-3-phenylpropanamido]acetamido}methoxy) acetate (5.00 g; 6.97 mmol; 37.9 %; off white solid; Purified Product).

LC/MS Chromatography: Column: ATLANTIS dC18 (50x4.6 mm) 5 µm; Mobile phase: A:0.1% HCOOH in H_2O:ACN(95:5) B: ACN; Flow Rate :1.5 mL/min: [M+Na]+ = 670, RT = 2.15 min.

Step 4:

To a stirred solution of benzyl benzyl 2-({2-[(2S)-2-[2-(2-{[(benzyloxy)carbonyl]amino}acetamido) acetamido]-3-phenylpropanamido]acetamido}methoxy)acetate (5.00 g; 6.97 mmol; 1.00 eq.) in DMF (50.00 mL; 10.00 V) was added Palladium on carbon (10% w/w) (4.00 g; 3.76 mmol; 0.54 eq.) and stirred at RT under hydrogen bladder pressure for 6 h.

After completion, reaction mixture was filtered through celite bed and washed the celite bed with mixture of THF and water (100 : 50) and concentrated, the obtained crude product was co-evaporated with toluene twice and dried to afford 2-({2-[(2S)-2-[2-(2-aminoacetamido)acetamido]-3-phenylpropanamido]acetamido}methoxy)acetic acid (2.50 g; 5.20 mmol; 74.7 %; off white solid; Crude Product).

LC/MS Chromatography: Column: ATLANTIS dC18 (50x4.6 mm) 5 µm; Mobile phase: A:0.1% HCOOH in H_2O:ACN(95:5) B: ACN; Flow Rate :1.5 mL/min: [M+H]+ = 424, RT = 0.87 min.

Step 5:

To a stirred solution of 2-({2-[(2S)-2-[2-(2-aminoacetamido)acetamido]-3-phenylpropanamido] acetamido} methoxy)acetic acid (2.50 g; 5.21 mmol; 1.00 eq.) in DMF (50.00 mL; 20.00 V) was added 6-(2,5-Dioxo-2,5-dihydro-pyrrol-1-yl)-hexanoic acid 2,5-dioxo-pyrrolidin-1-yl ester (2.00 g; 6.42 mmol; 1.23 eq.) and followed by Triethyl-amine (0.82 mL; 5.82 mmol; 1.12 eq.) at 0°C and stirred at RT for 2 h.

After completion of the reaction, reaction mass was concentrated to dryness to afford crude product. The crude product was purified by reverse phase column chromatoghraphy eluent at 30% of 0.1% HCOOH in water and ACN, the collected

fractions were lyophilized to afford pure product 2-({2-[(2S)-2-(2-{2-[6-(2,5-dioxo-2,5-dihydro-1H-pyrrol-1-yl)hexanamido]acetamido}acetamido)-3-phenylpropanamido]acetamido}methoxy)acetic acid (1.90 g; 3.04 mmol; 58.4 %; off white solid; Purified Product).

LC/MS Chromatography: Column: ATLANTIS dC18 (50x4.6 mm) 5 µm; Mobile phase: A:0.1% HCOOH in H_2O:ACN(95:5) B: ACN; Flow Rate :1.5 mL/min: [M-H]- = 615, RT = 1.51 min.

^{1}H NMR: 400 MHz, DMSO-d6:12.80 (s, 1H), 8.57 (t, J = 13.20 Hz, 1H), 8.31 (t, J = 11.60 Hz, 1H), 8.15-8.01 (m, 3H), 7.28-7.16 (m, 5H), 7.01 (s, 2H), 4.61 (d, J = 6.80 Hz, 2H), 4.50-4.50 (m, 1H), 3.98 (s, 1H), 3.77-3.66 (m, 6H), 3.57-3.34 (m, 1H), 2.81-2.80 (m, 1H), 2.12 (t, J = 7.20 Hz, 2H), 1.51-1.47 (m, 4H), 1.21-1.17 (m, 2H).

Step 6:

2-({2-[(2S)-2-(2-{2-[6-(2,5-dioxo-2,5-dihydro-1H-pyrrol-1-yl)hexanamido]acetamido}acetamido)-3-phenylpropanamido]acetamido}methoxy)acetic acid (427.38 mg; 0.66 mmol; 1.00 eq.) was dissolved in N,N-Dimethylformamide for spectroscopy Uvasol® (2.00 mL). HATU (185.89 mg; 0.79 mmol; 1.20 eq.) was added and the solution was stirred at RT 30 min. Then exatecan methanesulfonic acid (350.00 mg; 0.66 mmol; 1.00 eq.) and 4-Methylmorpholine for synthesis (144.78 µL; 1,32 mmol; 2.00 eq.) were added and the solution was stirred at RT overnight. The reaction solution was injected directly onto the column of the prep. HPLC and the fractions containing product were combined and lyophilized afford Maleimide-GGFG-DXd (220 mg; 0.21 mmol; 32 %; pure product, yellow solid).

LC/MS Chromatography: Column: ATLANTIS dC18 (50x4.6 mm) 5 µm; Mobile phase: A:0.1% HCOOH in H_2O:ACN(95:5) B: ACN; Flow Rate :1.5 mL/min: [M+H]+ = 1034, RT = 0.87 min.

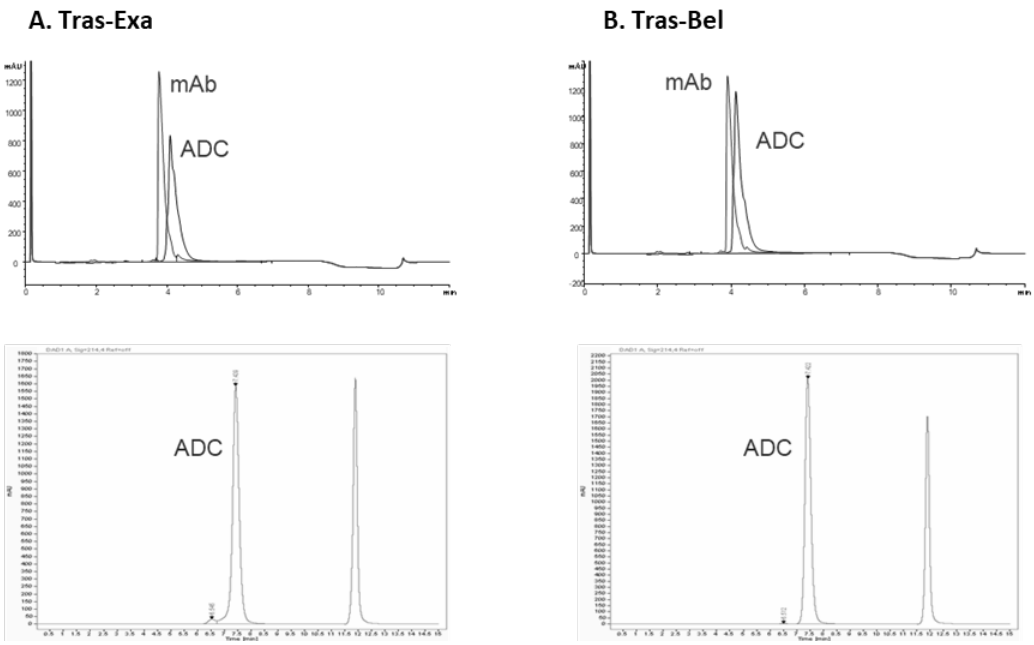

Figure S27a. RP-HPLC overlays (upper panel) and SE-HPLC (lower panel) chromatograms of non-reduced Tras-Exa **(A)** and Tras-Bel **(B)**. Signals were recorded at 214 nm.

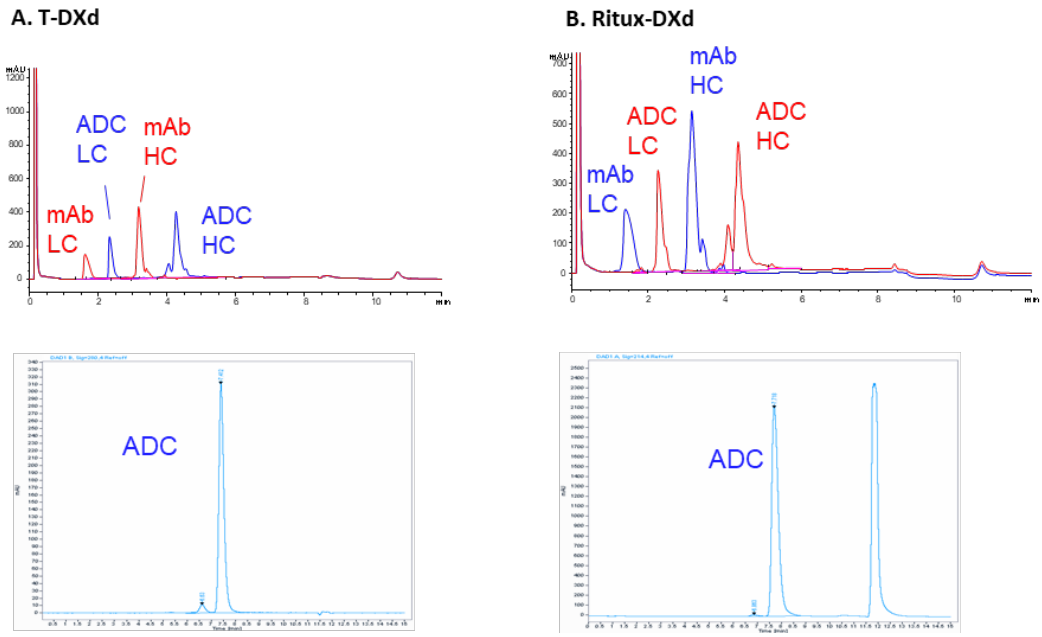

Figure S27b. RP-HPLC overlays (upper panel) and SE-HPLC (lower panel) chromatograms of T-DXd **(A)** and Ritux-DXd **(B)**. Since the thiol conjugation process results in depletion of interchain disulfide bonds, all samples were reduced prior to RP-HPLC analysis and therefore separated into heavy chains (HC) and light chains (LC). Signal for SE-HPLC of T-DXd was recorded at 280 nm, all other signals were recorded at 214 nm.

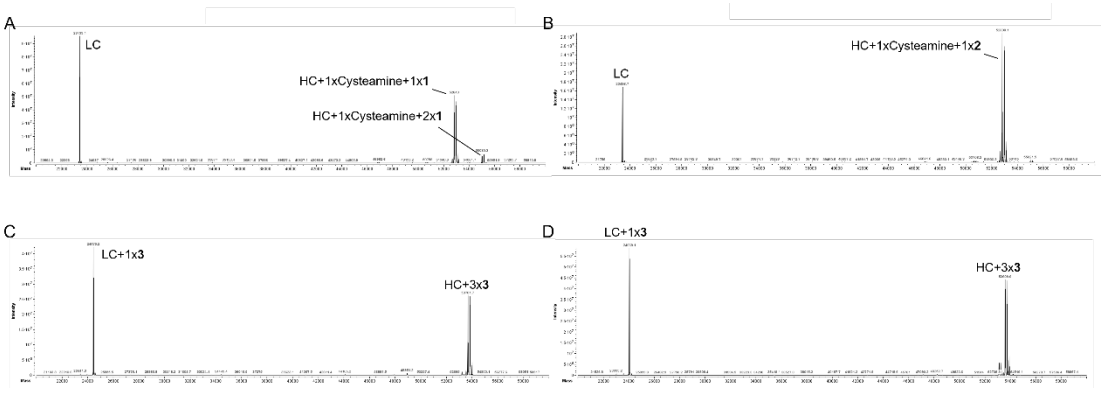

Figure S27c. LC-MS spectra of Tras-Exa **(A)**, Tras-Bel **(B)**, T-DXd **(C)** and Ritux-DXd **(D)**. All samples were reduced prior to LC-MS analysis and therefore separated into heavy chains (HC) and light chains (LC). Multiple peaks were detected for the heavy chains due to different glycosylated species. Heavy chains of Tras-Exa **(A)** and Tras-Bel **(B)** were conjugated with cysteamine serving as a handle for the attachment of **1** or **2** resulting in DARs 4.3 and 3.9, respectively. For T-DXd **(C)** and Ritux-DXd **(D)**, **3** was conjugated to the mAb interchain cysteines resulting in attachment of one molecule to each LC and three to each HC (overall DARs of 7.9 and 8.0, respectively).

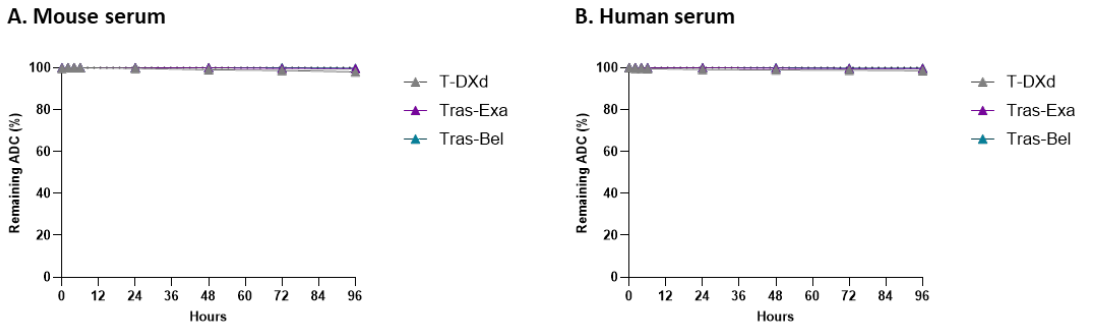

Figure S28. Drug-linker stability. Percentage of ADC remaining over time in mouse (A) and human (B) sera following incubation at 37°C for 96 h, calculated from free exatecan, belotecan or DXd that were measured via LC-MS/MS. Numbers show the released fraction (%) relative to initially conjugated payload.

Serum Stability

Serum samples from mice and humans were purchased from Biowest. Serum was thawed at ambient temperature and supplemented with 2 M HEPES buffer (Merck KGaA, Darmstadt), pH 7.55 in order to obtain a 0.3 M final HEPES concentration. Supplementation was performed in order to maintain serum pH levels close to physiological pH ranging between pH 7.3 and 7.4. Buffered serum was filtered through a 0.22 µm filter (Merck KGaA, Darmstadt). ADC stock solutions were added to the plasma samples at final concentration of 50 µg ADC protein/mL, mixed and transferred to PCR tubes (Thermo Fisher Scientific) with a final volume of 20 µL per aliquot and followed by incubation at 37°C in a CO_2 incubator. Triplicates were prepared for each sample. Sample time series were collected at timepoints 0, 2, 4, 6, 24, 48, 72 and 96 h and stored at -80°C until further analysis. ADC serum samples were transferred to PCR tubes (5 µL) and supplemented with internal standard, followed by extraction with 150 µL methanol and analysis of exatecan by UPLC MS/MS. For the UPLC system, the ACQUITY UPLC H-Class System (Waters) was used along with the ACQUITY UPLC BEH C18 1.7 µm 2.1 x 50 mm column (Waters). For the mobile phase, solvent A was used with 0.1% formic acid in H_2O and acetonitrile for solvent B. Mass spectrometer measurements were performed using a Sciex Triple Quad 6500 system (AB Sciex) and ABSciex Analyst 1.7 software for data analysis.

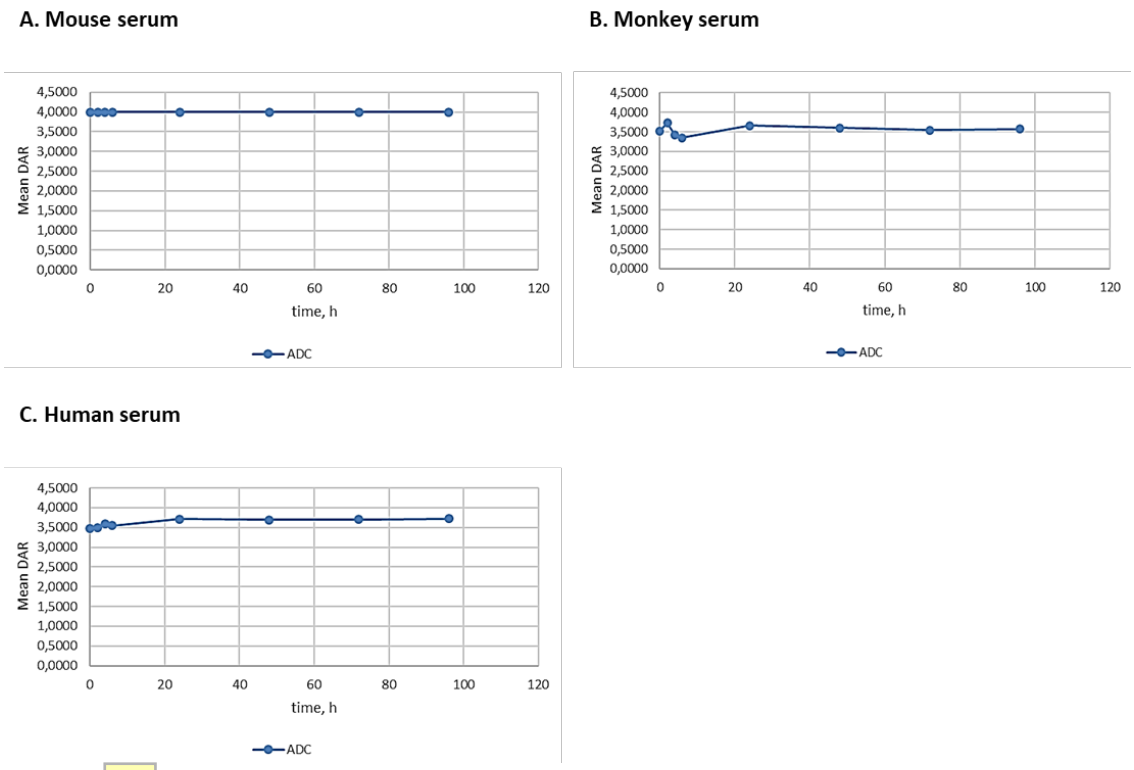

Figure S29 Drug-linker stability. Mean DAR of ADC over time in mouse serum **(A)**, monkey serum **(B)** and human serum **(C)** was determined by UPLC MS/MS.

REFERENCES

(1) Van Cutsem, E.; Sagaert, X.; Topal, B.; Haustermans, K.; Prenen, H. Gastric cancer. *Lancet* **2016**, *388* (10060), 2654-2664. DOI: 10.1016/S0140-6736(16)30354-3.

(2) Onitilo, A. A.; Engel, J. M.; Greenlee, R. T.; Mukesh, B. N. Breast cancer subtypes based on ER/PR and Her2 expression: comparison of clinicopathologic features and survival. *Clin Med Res* **2009**, *7* (1-2), 4-13. DOI: 10.3121/cmr.2009.825.

(3) Waks, A. G.; Winer, E. P. Breast Cancer Treatment: A Review. *JAMA* **2019**, *321* (3), 288-300. DOI: 10.1001/jama.2018.19323 From NLM Medline.

(4) Yarden, Y.; Sliwkowski, M. X. Untangling the ErbB signalling network. *Nat Rev Mol Cell Biol* **2001**, *2* (2), 127-137. DOI: 10.1038/35052073 From NLM Medline.

(5) Slamon, D. J.; Leyland-Jones, B.; Shak, S.; Fuchs, H.; Paton, V.; Bajamonde, A.; Fleming, T.; Eiermann, W.; Wolter, J.; Pegram, M.; et al. Use of chemotherapy plus a monoclonal antibody against HER2 for metastatic breast cancer that overexpresses HER2. *N Engl J Med* **2001**, *344* (11), 783-792. DOI: 10.1056/NEJM200103153441101.

(6) Seidman, A.; Hudis, C.; Pierri, M. K.; Shak, S.; Paton, V.; Ashby, M.; Murphy, M.; Stewart, S. J.; Keefe, D. Cardiac dysfunction in the trastuzumab clinical trials experience. *J Clin Oncol* **2002**, *20* (5), 1215-1221. DOI: 10.1200/JCO.2002.20.5.1215 From NLM Medline.

(7) Gajria, D.; Chandarlapaty, S. HER2-amplified breast cancer: mechanisms of trastuzumab resistance and novel targeted therapies. *Expert Rev Anticancer Ther* **2011**, *11* (2), 263-275. DOI: 10.1586/era.10.226 From NLM Medline.

(8) Zhong, L.; Li, Y.; Xiong, L.; Wang, W.; Wu, M.; Yuan, T.; Yang, W.; Tian, C.; Miao, Z.; Wang, T.; et al. Small molecules in targeted cancer therapy: advances, challenges, and future perspectives. *Signal Transduct Target Ther* **2021**, *6* (1), 201. DOI: 10.1038/s41392-021-00572-w.

(9) Scott, A. M.; Wolchok, J. D.; Old, L. J. Antibody therapy of cancer. *Nat Rev Cancer* **2012**, *12* (4), 278-287. DOI: 10.1038/nrc3236 From NLM Medline.

(10) Fu, Z.; Li, S.; Han, S.; Shi, C.; Zhang, Y. Antibody drug conjugate: the "biological missile" for targeted cancer therapy. *Signal Transduct Target Ther* **2022**, *7* (1), 93. DOI: 10.1038/s41392-022-00947-7 From NLM Medline.

(11) Amiri-Kordestani, L.; Blumenthal, G. M.; Xu, Q. C.; Zhang, L.; Tang, S. W.; Ha, L.; Weinberg, W. C.; Chi, B.; Candau-Chacon, R.; Hughes, P.; et al. FDA approval: ado-trastuzumab emtansine for the treatment of patients with HER2-positive metastatic breast cancer. *Clin Cancer Res* **2014**, *20* (17), 4436-4441. DOI: 10.1158/1078-0432.CCR-14-0012 From NLM Medline.

(12) *FDA approves ado-trastuzumab emtansine for early breast cancer*. 2019. https://www.fda.gov/drugs/resources-information-approved-drugs/fda-approves-ado-trastuzumab-emtansine-early-breast-cancer (accessed.

(13) Narayan, P.; Osgood, C. L.; Singh, H.; Chiu, H. J.; Ricks, T. K.; Chiu Yuen Chow, E.; Qiu, J.; Song, P.; Yu, J.; Namuswe, F.; et al. FDA Approval Summary: Fam-Trastuzumab Deruxtecan-Nxki for the Treatment of Unresectable or Metastatic HER2-Positive Breast Cancer. *Clin Cancer Res* **2021**, *27* (16), 4478-4485. DOI: 10.1158/1078-0432.CCR-20-4557 From NLM Medline.

(14) *FDA approves fam-trastuzumab deruxtecan-nxki for HER2-positive gastric adenocarcinomas*. 2021. https://www.fda.gov/drugs/resources-information-approved-drugs/fda-approves-fam-trastuzumab-deruxtecan-nxki-her2-positive-gastric-adenocarcinomas (accessed.

(15) *FDA Approves First Targeted Therapy for HER2-Low Breast Cancer*. 2022. https://www.fda.gov/news-events/press-announcements/fda-approves-first-targeted-therapy-her2-low-breast-cancer (accessed.
(16) *FDA grants accelerated approval to fam-trastuzumab deruxtecan-nxki for HER2-mutant non-small cell lung cancer*. 2022. https://www.fda.gov/drugs/resources-information-approved-drugs/fda-grants-accelerated-approval-fam-trastuzumab-deruxtecan-nxki-her2-mutant-non-small-cell-lung (accessed.
(17) Sievers, E. L.; Senter, P. D. Antibody-drug conjugates in cancer therapy. *Annu Rev Med* **2013**, *64*, 15-29. DOI: 10.1146/annurev-med-050311-201823.
(18) McCombs, J. R.; Owen, S. C. Antibody drug conjugates: design and selection of linker, payload and conjugation chemistry. *AAPS J* **2015**, *17* (2), 339-351. DOI: 10.1208/s12248-014-9710-8.
(19) Tsuchikama, K.; An, Z. Antibody-drug conjugates: recent advances in conjugation and linker chemistries. *Protein Cell* **2018**, *9* (1), 33-46. DOI: 10.1007/s13238-016-0323-0 From NLM Medline.
(20) Junutula, J. R.; Raab, H.; Clark, S.; Bhakta, S.; Leipold, D. D.; Weir, S.; Chen, Y.; Simpson, M.; Tsai, S. P.; Dennis, M. S.; et al. Site-specific conjugation of a cytotoxic drug to an antibody improves the therapeutic index. *Nat Biotechnol* **2008**, *26* (8), 925-932. DOI: 10.1038/nbt.1480 From NLM Medline.
(21) Bargh, J. D.; Isidro-Llobet, A.; Parker, J. S.; Spring, D. R. Cleavable linkers in antibody-drug conjugates. *Chem Soc Rev* **2019**, *48* (16), 4361-4374. DOI: 10.1039/c8cs00676h From NLM Medline.
(22) Beck, A.; Goetsch, L.; Dumontet, C.; Corvaia, N. Strategies and challenges for the next generation of antibody-drug conjugates. *Nat Rev Drug Discov* **2017**, *16* (5), 315-337. DOI: 10.1038/nrd.2016.268 From NLM Medline.
(23) Gondi, C. S.; Rao, J. S. Cathepsin B as a cancer target. *Expert Opin Ther Targets* **2013**, *17* (3), 281-291. DOI: 10.1517/14728222.2013.740461.
(24) Dickgiesser, S.; Rieker, M.; Mueller-Pompalla, D.; Schroter, C.; Tonillo, J.; Warszawski, S.; Raab-Westphal, S.; Kuhn, S.; Knehans, T.; Konning, D.; et al. Site-Specific Conjugation of Native Antibodies Using Engineered Microbial Transglutaminases. *Bioconjug Chem* **2020**, *31* (4), 1070-1076. DOI: 10.1021/acs.bioconjchem.0c00061 From NLM Medline.
(25) Lyon, R. P.; Meyer, D. L.; Setter, J. R.; Senter, P. D. Conjugation of anticancer drugs through endogenous monoclonal antibody cysteine residues. *Methods Enzymol* **2012**, *502*, 123-138. DOI: 10.1016/B978-0-12-416039-2.00006-9 From NLM Medline.
(26) Jager, S.; Wagner, T. R.; Rasche, N.; Kolmar, H.; Hecht, S.; Schroter, C. Generation and Biological Evaluation of Fc Antigen Binding Fragment-Drug Conjugates as a Novel Antibody-Based Format for Targeted Drug Delivery. *Bioconjug Chem* **2021**, *32* (8), 1699-1710. DOI: 10.1021/acs.bioconjchem.1c00240 From NLM Medline.
(27) Kaempffe, A.; Dickgiesser, S.; Rasche, N.; Paoletti, A.; Bertotti, E.; De Salve, I.; Sirtori, F. R.; Kellner, R.; Konning, D.; Hecht, S.; et al. Effect of Conjugation Site and Technique on the Stability and Pharmacokinetics of Antibody-Drug Conjugates. *J Pharm Sci* **2021**, *110* (12), 3776-3785. DOI: 10.1016/j.xphs.2021.08.002 From NLM Medline.

(28) Amir, R. J.; Pessah, N.; Shamis, M.; Shabat, D. Self-immolative dendrimers. *Angew Chem Int Ed Engl* **2003**, *42* (37), 4494-4499. DOI: 10.1002/anie.200351962 From NLM PubMed-not-MEDLINE.
(29) Haba, K.; Popkov, M.; Shamis, M.; Lerner, R. A.; Barbas, C. F., 3rd; Shabat, D. Single-triggered trimeric prodrugs. *Angew Chem Int Ed Engl* **2005**, *44* (5), 716-720. DOI: 10.1002/anie.200461657 From NLM Medline.
(30) Shamis, M.; Lode, H. N.; Shabat, D. Bioactivation of self-immolative dendritic prodrugs by catalytic antibody 38C2. *J Am Chem Soc* **2004**, *126* (6), 1726-1731. DOI: 10.1021/ja039052p From NLM Medline.
(31) Gopin, A.; Ebner, S.; Attali, B.; Shabat, D. Enzymatic activation of second-generation dendritic prodrugs: Conjugation of self-immolative dendrimers with poly(ethylene glycol) via click chemistry. *Bioconjug Chem* **2006**, *17* (6), 1432-1440. DOI: 10.1021/bc060180n.
(32) Anami, Y.; Yamazaki, C. M.; Xiong, W.; Gui, X.; Zhang, N.; An, Z.; Tsuchikama, K. Glutamic acid-valine-citrulline linkers ensure stability and efficacy of antibody-drug conjugates in mice. *Nat Commun* **2018**, *9* (1), 2512. DOI: 10.1038/s41467-018-04982-3 From NLM Medline.
(33) McDermott, M. S. J.; Sharko, A. C.; Munie, J.; Kassler, S.; Melendez, T.; Lim, C. U.; Broude, E. V. CDK7 Inhibition is Effective in all the Subtypes of Breast Cancer: Determinants of Response and Synergy with EGFR Inhibition. *Cells* **2020**, *9* (3). DOI: 10.3390/cells9030638.
(34) Gu, S.; Hu, Z.; Ngamcherdtrakul, W.; Castro, D. J.; Morry, J.; Reda, M. M.; Gray, J. W.; Yantasee, W. Therapeutic siRNA for drug-resistant HER2-positive breast cancer. *Oncotarget* **2016**, *7* (12), 14727-14741. DOI: 10.18632/oncotarget.7409.
(35) Lehmann, B. D.; Bauer, J. A.; Chen, X.; Sanders, M. E.; Chakravarthy, A. B.; Shyr, Y.; Pietenpol, J. A. Identification of human triple-negative breast cancer subtypes and preclinical models for selection of targeted therapies. *J Clin Invest* **2011**, *121* (7), 2750-2767. DOI: 10.1172/JCI45014.
(36) Aggarwal, N.; Sloane, B. F. Cathepsin B: multiple roles in cancer. *Proteomics Clin Appl* **2014**, *8* (5-6), 427-437. DOI: 10.1002/prca.201300105 From NLM Medline.
(37) Mahalingaiah, P. K.; Ciurlionis, R.; Durbin, K. R.; Yeager, R. L.; Philip, B. K.; Bawa, B.; Mantena, S. R.; Enright, B. P.; Liguori, M. J.; Van Vleet, T. R. Potential mechanisms of target-independent uptake and toxicity of antibody-drug conjugates. *Pharmacol Ther* **2019**, *200*, 110-125. DOI: 10.1016/j.pharmthera.2019.04.008 From NLM Medline.
(38) Singh, A. P.; Guo, L.; Verma, A.; Wong, G. G.; Shah, D. K. A Cell-Level Systems PK-PD Model to Characterize In Vivo Efficacy of ADCs. *Pharmaceutics* **2019**, *11* (2). DOI: 10.3390/pharmaceutics11020098 From NLM PubMed-not-MEDLINE.
(39) Danieli, E.; Shabat, D. Molecular probe for enzymatic activity with dual output. *Bioorg Med Chem* **2007**, *15* (23), 7318-7324. DOI: 10.1016/j.bmc.2007.08.046.
(40) Amir, R. J.; Danieli, E.; Shabat, D. Receiver-amplifier, self-immolative dendritic device. *Chemistry* **2007**, *13* (3), 812-821. DOI: 10.1002/chem.200601263.
(41) Roth-Konforti, M. E.; Bauer, C. R.; Shabat, D. Unprecedented Sensitivity in a Probe for Monitoring Cathepsin B: Chemiluminescence Microscopy Cell-Imaging of a Natively Expressed Enzyme. *Angew Chem Int Ed Engl* **2017**, *56* (49), 15633-15638. DOI: 10.1002/anie.201709347.

(42) Gromek, S. M.; deMayo, J. A.; Maxwell, A. T.; West, A. M.; Pavlik, C. M.; Zhao, Z.; Li, J.; Wiemer, A. J.; Zweifach, A.; Balunas, M. J. Synthesis and biological evaluation of santacruzamate A analogues for anti-proliferative and immunomodulatory activity. *Bioorg Med Chem* **2016**, *24* (21), 5183-5196. DOI: 10.1016/j.bmc.2016.08.040.
(43) Roussakis, E.; Li, Z.; Nowell, N. H.; Nichols, A. J.; Evans, C. L. Bright, "Clickable" Porphyrins for the Visualization of Oxygenation under Ambient Light. *Angew Chem Int Ed Engl* **2015**, *54* (49), 14728-14731. DOI: 10.1002/anie.201506847.
(44) Bachl, J.; Mayr, J.; Sayago, F. J.; Cativiela, C.; Díaz Díaz, D. Amide-triazole isosteric substitution for tuning self-assembly and incorporating new functions into soft supramolecular materials. *Chem Commun (Camb)* **2015**, *51* (25), 5294-5297. DOI: 10.1039/c4cc08593k.